Complexity of frequency receptive fields predicts tonotopic variability across species

Quentin Gaucher[1*], Mariangela Panniello[1*], Aleksandar Z Ivanov[1], Johannes C Dahmen[1], Andrew J King[1], Kerry M M Walker[1,2]

[1] Dept of Physiology, Anatomy & Genetics, University of Oxford

Sherrington Building, Parks Road, Oxford, OX1 3PT, UK

[2] Corresponding author: kerry.walker@dpag.ox.ac.uk

[*] These authors contributed equally to this work

Keywords: auditory cortex, tonotopy, two-photon calcium imaging, ferret, mouse, frequency, maps

Abstract

Primary cortical areas contain maps of sensory features, including sound frequency in primary auditory cortex (A1). Two-photon calcium imaging in mice has confirmed the presence of these large-scale maps, while uncovering an unexpected local variability in the stimulus preferences of individual neurons in A1 and other primary regions. Here we show that fractured tonotopy is not unique to rodents. Using two-photon imaging, we found that local variance in frequency preferences is equivalent in ferrets and mice. Much of this heterogeneity was due to neurons with complex frequency tuning, which are less spatially organized than those tuned to a single frequency. Finally, we show that microelectrode recordings may describe a smoother tonotopic arrangement due to a bias towards neurons with simple frequency tuning. These results show that local variability in the tonotopic map is not restricted to rodents and help explain inconsistencies in cortical topography across species and recording techniques.

Introduction

The primary sensory areas of the cerebral cortex are characterized by a systematic spatial arrangement of responses to the stimulus features represented by peripheral receptors. In A1, this takes the form of a logarithmic gradient of neural response preferences for a single "best" frequency, known as tonotopy[1].

Early electrophysiological investigations revealed a tonotopic arrangement of neuronal frequency preferences in A1 in all species studied, including monkeys[2], cats[3], ferrets[4], gerbils[5], and rats[6]. More recent multielectrode recordings[7–9] and large-scale imaging experiments[10] have confirmed the presence of a tonotopic gradient over large areas of A1 in carnivores and primates, while single-neuron recordings in awake animals have reported clear frequency gradients in marmosets[11] and weak tonotopy in cats[12].

In vivo two-photon calcium imaging can measure the stimulus preferences of a much larger number of individual neurons within a cortical region than the above techniques, improving the spatial sampling of mapping studies. The results of such experiments in mouse A1 over the past decade have challenged our understanding of the cortical tonotopic map. While previous electrophysiological and large-scale imaging reports confirmed an overall tonotopic organization in mouse A1[13–15], most two-photon imaging studies have shown that, at the more local scale, neighboring neurons vary widely in their frequency preferences[16–20]. Similarly, two-photon imaging has demonstrated local heterogeneity in whisker selectivity in mouse primary somatosensory cortex[21,22], and in orientation tuning in mouse primary visual cortex (V1)[23].

There are several possible explanations for the local variation of A1 frequency preferences revealed by two-photon imaging studies compared to the smoother tonotopy described in electrophysiological studies. First, the heterogeneity may be due to the higher spatial sampling rate of two-photon imaging. Microelectrode studies are often based on responses that are summed across several neurons, and this spatial averaging may lead to smoother tonotopic gradients[14]. Even when microelectrode data are

restricted to single neuron recordings, the spacing between neurons is typically ~100 μm or greater, so local variations in stimulus preferences cannot be examined[24]. Second, multielectrode recordings may be biased more towards the most robustly responding neurons in granular layers that receive direct thalamic input, whereas most two-photon imaging studies have been restricted to the superficial layers of the cortex[14,25]. However, Tischbirek et al. report similar tonotopic organization across all layers of mouse auditory cortex[26]. Third, the variations in tonotopy across studies may partly reflect a species difference in the cortical organization of rodents and higher mammals, particularly as local thalamic inputs to A1 in mice are also heterogeneous in their frequency tuning[27]. Two-photon studies of primary visual cortex have revealed poorer spatial organization of orientation tuning in rodents than in cats[23,28], tree shrews[29], and ferrets[30]. The same may be true of tonotopy in A1. This view is further supported by a recent study in marmosets, in which A1 was reported to be more tonotopically organized than in rats[31].

It is not clear how spatial organization of tuning to a single sound frequency coincides with the known functions and complex frequency receptive fields of auditory cortex. Throughout the ascending auditory pathway, neurons progressively integrate spectral and temporal features of sound[32], and the receptive fields of many A1 neurons are poorly predicted by a model of linear tuning to a single sound frequency[33,34]. Recent studies have shown that the preferred frequencies of weakly tuned A1 neurons are poorly mapped[20,26]. An outstanding question we address here is how neurons with reliable tuning to multiple frequency peaks impact on tonotopic organization.

The present experiments also examine whether local heterogeneity in tonotopy is a general feature of mammalian A1, or a peculiarity of rodents. We developed the first use of *in vivo* two-photon calcium imaging to examine the functional organization of A1 of ferrets. Ferrets are a popular animal model in auditory neuroscience, and their arrangement of orientation selectivity in V1 differs from that in rodents[23,30]. We found that mice and ferrets show comparable local heterogeneity of frequency preferences in well-tuned neurons. Furthermore, neurons with more complex frequency receptive fields have poorer tonotopic arrangement in both species. Our findings suggest that ferrets and mice

may use the same general principles for mapping frequency in A1, and explain past discrepancies in cortical maps described in studies using different species and experimental techniques.

Results

We investigated how the frequency preferences of neurons in the superficial layers of ferret A1 are organized spatially, both locally (within ~0.25 mm^2) and across the entire tonotopic axis (~3.5 mm), and how this organization compares to the fractured local tonotopy reported in mice[16,17,19]. We expressed GCaMP6 in the right A1 of 8 ferrets (Figure 1A; Figure 1-figure supplement 1A,B) and recorded neuronal calcium transients in 3640 neurons across 32 imaging fields (e.g. Figure 1A,B), while presenting pure tones (0.3 - 41 kHz; 30 – 90 dB SPL) to the contralateral ear. To ensure that our recordings were carried out in layers 2/3, we imaged neuronal activity at 176 ± 26.83 μm (median ± SD) below the cortical surface (Figure 1-figure supplement 2).

Frequency response organization at the local scale

Across all fields imaged in ferret A1, 693 of 3604 (19.23%) neurons were frequency-sensitive (two-way ANOVA; $p < 0.05$). Neurons often showed a V-shaped Frequency Response Area (FRA; Figure 1B), with a clearly defined Best Frequency (BF). In this example field (300 x 300 μm), 26.5% of neurons were significantly sensitive to tone frequency or frequency/level combinations, and the average BF across all frequency-sensitive neurons (Figure 1C) was 14.7 kHz (± 0.75 kHz; mean ± SEM). As previously described for A1 of mice[16,17,19], most neurons within this local region of ferret A1 were tuned to a similar BF, but there were some outliers preferring higher or lower BFs (Figure 1D). The BF of individual neurons in this field ranged from 2.2 kHz to 19.9 kHz, with 9% of BFs being more than one octave away from the mean.

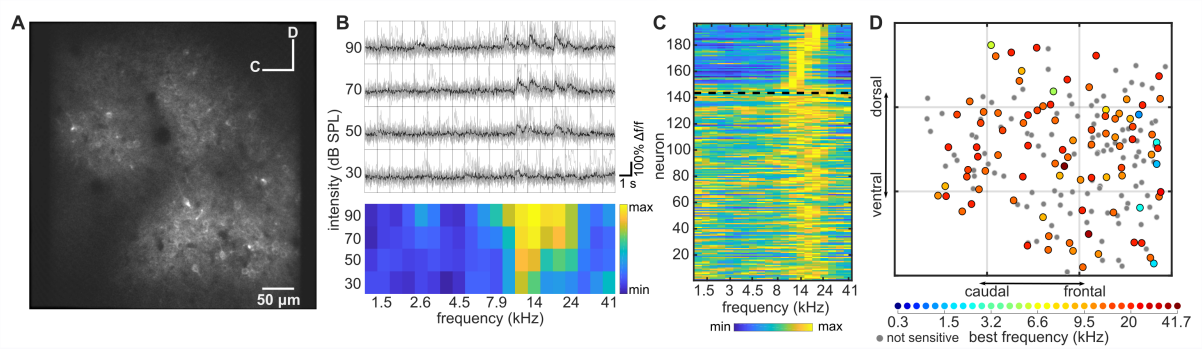

Figure 1. Imaging neuronal responses to pure tones in ferret A1. (A) An example cortical field in A1 of ferret 1, imaged 120 µm below the pial surface. **(B)** Responses of one neuron in **(A)** to pure tones presented at different frequencies and sound levels. Top panel: single trial (grey) and trial-averaged (black) $\Delta F/F_0$ traces, measured for 1 s from sound onset. Bottom panel: Frequency Response Area (FRA) of the same neuron. Color scale indicates the trial-averaged response of the neuron to tones presented at each frequency/level combination, calculated from the deconvolved fluorescence trace (see Methods). **(C)** Level-averaged tuning curves of all neurons in **(A)**. Neurons above the dotted black line were significantly modulated by frequency (two-way ANOVA, $p < 0.05$) and are sorted by their Best Frequency (BF). Neurons below the line were not sensitive to sound frequency and are sorted by the p-value of the frequency predictor in the two-way ANOVA (bottom neurons have the largest p-value). **(D)** Map of the neurons in **(A)** color-coded according to their BF (see colour scale below). Grey dots represent neurons that were not sensitive to tone frequency. Each grey square is 100 µm^2.

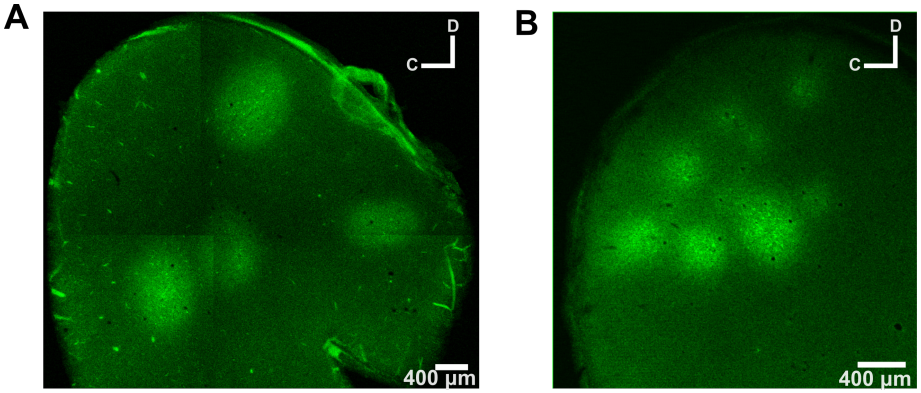

Figure 1-figure supplement 1. GCaMP6 expression in ferret auditory cortex. Tangential sections of the auditory cortex are shown to visualize the locations and spread of GCaMP6 injections. Sections were 50 µm thick and were acquired at 200 µm below the cortical surface. **(A)** The auditory cortex of ferret 3 was injected with a 1:1 solution of AAV1.Syn.GCaMP6f.P2A-nls-dTomato.WPRE.SV40 and AAV1.mDlx.GFP-GCaMP6f-Fishell-2.WPRE.SV40 in four cortical locations. The typical spread of these injections was ~800 µm in diameter per site. **(B)** Auditory cortex shown as in **(A)**, but for ferret 7. Here, a 1:1 solution of AAV1.Syn.GCaMP6m.WPRE.SV40 and PBS was injected at seven injection sites, and the typical spread was ~400 µm in diameter per site.

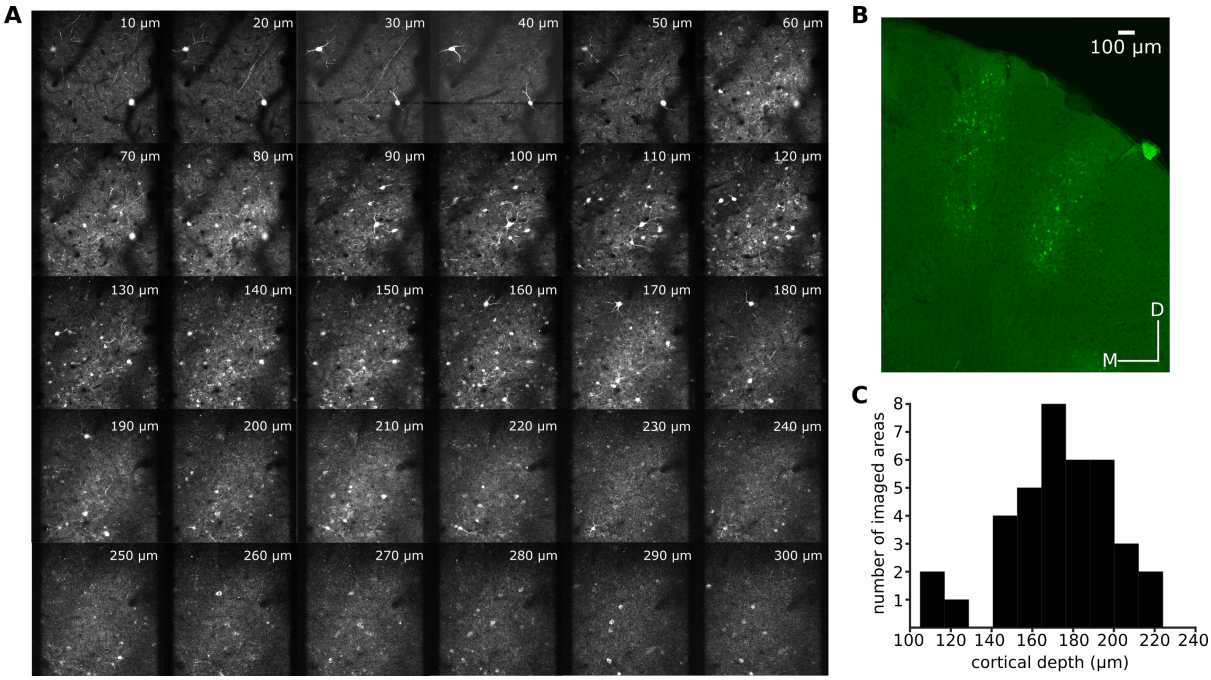

Figure 1-figure supplement 2. Imaging in layer 2/3 of ferret A1. (A) A series of z-projections acquired *in vivo* using two-photon imaging in ferret 7. The projections have the same fronto-caudal and dorso-ventral axis as the imaged field shown in Figure 1A. Projections were selected to show 10 µm increments in cortical depth. While imaging, the most superficial neuronal bodies were visible ~60 µm below the cortical surface. **(B)** A coronal section of the A1 of ferret 4 showing the extent of GCaMP6 labeling throughout the cortical depth. **(C)** Distribution of the number of fields imaged at each cortical depth.

The practice of assigning a BF is based on the assumption that the neuron is tuned to a single preferred frequency, but the FRAs of auditory cortical neurons are not always "V-shaped"[8,13,35]. We observed that the FRAs of frequency-sensitive neurons in our ferret A1 dataset could be classified into three broad types: 1) V-, I- or O-shaped FRAs, which all have a clear single BF ("single-peaked neurons"); 2) FRAs with response peaks at two distinct frequencies ("double-peaked neurons"), where one peak is usually substantially stronger than the other; and 3) more complex FRAs, often containing three response peaks and a poorly defined BF. Little is known about the functions of neurons with these different frequency response profiles and their local spatial distribution has not been directly investigated, although neurons with multi-peaked FRAs have been reported in the A1 of marmosets[36] and rats[37]. We hypothesized that complexity in the shape of FRAs could help explain some of the reported local variability in cortical tonotopy, as it is less clear where double-peaked and complex FRAs should be located on a tonotopic map.

Each frequency-sensitive neuron was classified using an automated algorithm as having a single-peaked, double-peaked or complex FRA (see Methods; Figure 2A). In most imaging fields, we observed all three FRA classes, (as illustrated in Figure 2B), and the following analyses were restricted to imaging fields containing at least three neurons of each class. BF was derived in the same manner for neurons across all three classes, as the peak of the frequency response curve.

Visual inspection of tonotopic maps (Figure 2B; Figure 2-figure supplement 1) suggested that the BFs of double-peaked (BF_d) and complex neurons (BF_c) may be more varied within a local field than those of single-peaked neurons (BF_s). To quantitatively compare the local tonotopic organization of neurons with single-peaked, double-peaked and complex FRAs, we computed a BF variance metric. This metric was defined as the octave difference per millimeter between the BF of each neuron and the average BF of all other neurons in the imaging field.

Best frequencies varied less within an imaging field among single-peaked neurons (1.5 ± 0.11 octaves; mean ± SEM) than among double-peaked neurons (2.15 ± 0.17 octaves; t-test; $t = 5.25$, $p = 9.1 \times 10^{-7}$) and complex neurons (3.35 ± 0.23 octaves; $t = 8.47$, $p = 5.7 \times 10^{-16}$) (Figure 2C). Within double-peaked neurons, the frequency of the weaker second peak (peak 2) was more variable than that of BF_d ($t = 2.42$, $p = 0.016$). Therefore, tonotopic organization within a local region of ferret A1 is less reliable among neurons with more complex frequency receptive fields.

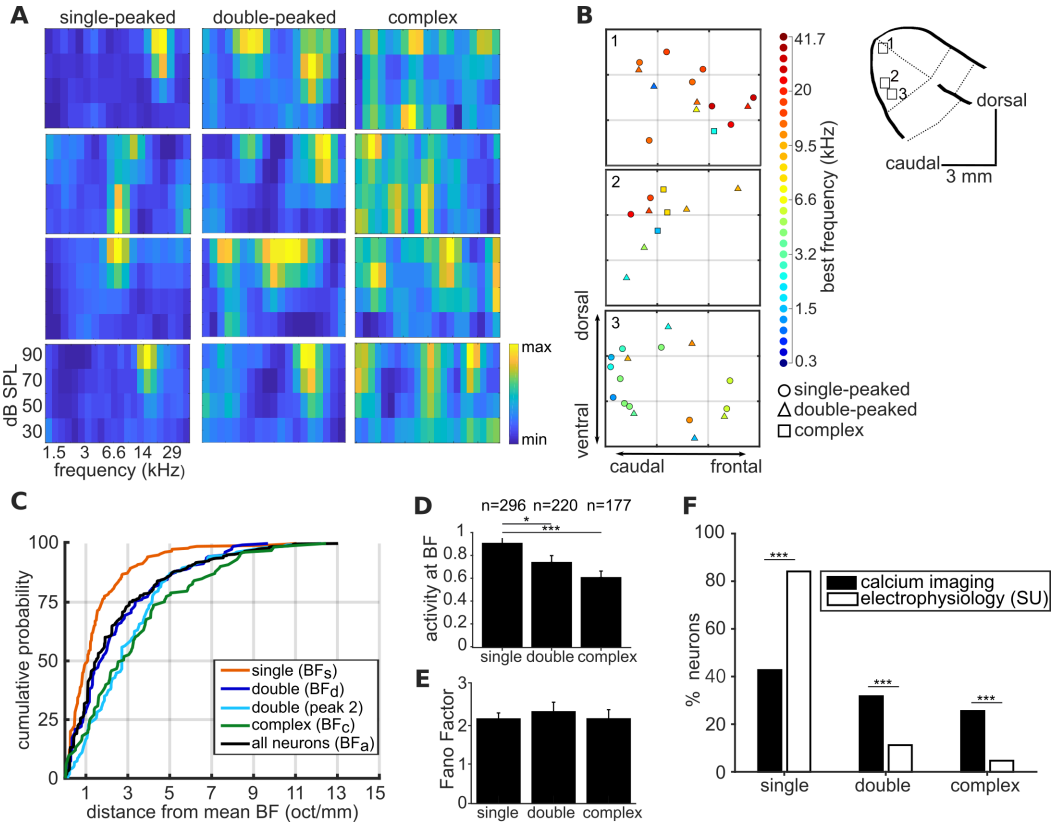

Figure 2. Complexity of frequency receptive fields predicts local variability in ferret A1 tonotopy. (A) FRA plots of four example neurons from ferret 6 for each of the three FRA classes. **(B)** Three 300 x 300 µm spatial maps of frequency-sensitive neurons along the tonotopic axis of ferret 6. Their anatomical locations within the ferret's ectosylvian gyrus are represented in the schematic to the right. The color of each neuron indicates its BF (see color scale, right), and the shape corresponds to the classification of its FRA. **(C)** Cumulative probability plots of the difference (in octaves) between each neuron's BF and the average BF of all neurons of the same FRA class in the same imaging field. Distributions for different FRA classes are plotted separately: single-peaked BF_s; double-peaked BF_d; double-peaked peak 2; complex BF_c; and the BF_a of all three FRAs together. **(D)** Magnitude of the trial-averaged response at BF, calculated from deconvolved fluorescence traces in two-photon imaging experiments. Responses were averaged across all neurons in each FRA class, pooled across imaging fields and ferrets (mean ± SEM). **(E)** Fano Factor values (mean ± SEM) for single-peaked, double-peaked, and complex neurons. **(F)** Percentage of neurons classified into each FRA class from two-photon calcium imaging (black) and single unit microelectrode recordings (white). The results of t-tests are indicated above the bars in **(D), (E)** and **(F)** (*$p < 0.05$ and *** $p < 0.001$).

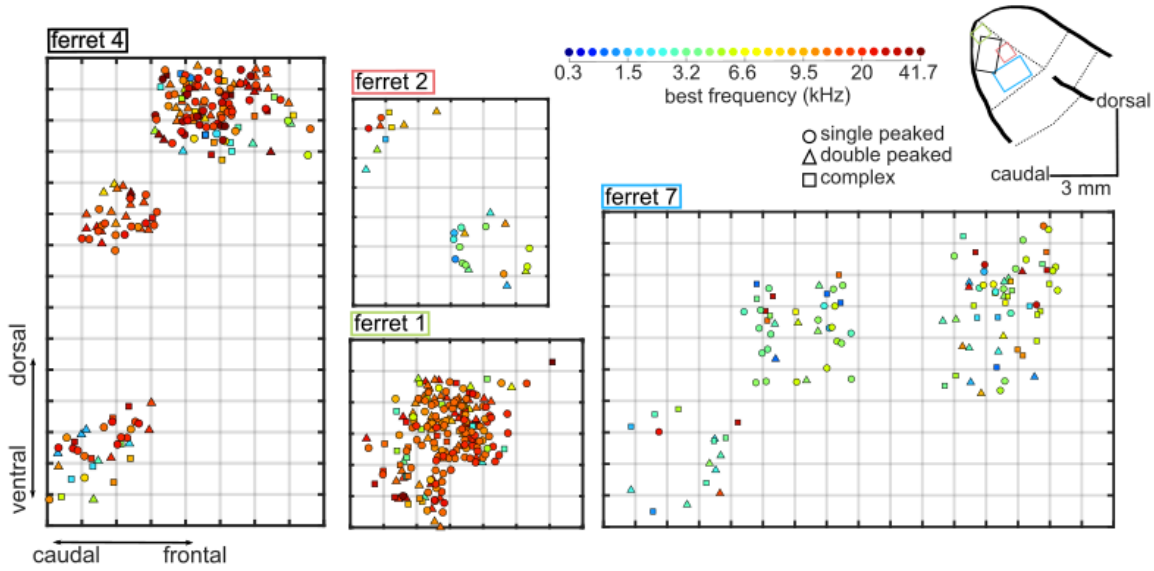

Figure 2-figure supplement 1. Spatial maps of best frequency in A1 of 4 ferrets. Each plot is a map of frequency-responsive neurons imaged in individual ferrets (ferrets 1, 2, 4 and 7). Neurons are plotted along the rostro-caudal and dorso-ventral axes. The color of each neuron indicates its BF, while the shape corresponds to the classification of its FRA (see colour scale, top center), as in Figure **2B**. Each grey grid in the maps corresponds to a cortical area of 100 x 100 µm. The locations of the four maps within A1 are represented on a common map of ferret auditory cortex as colored rectangles (top right, colour matches ferrets' numbers).

We also investigated whether the three classes of neurons differed in their response strengths (Figure 2D). We found that the average deconvolved calcium response at BF was stronger in single-peaked neurons compared to either double-peaked neurons (t-test; $t = 2.22$, $p = 0.027$) or neurons with complex FRAs ($t = 4.02$, $p = 6.93 \times 10^{-5}$). There was no significant difference in response strength between neurons with double-peaked and complex FRAs ($t = 1.58$, $p = 0.11$). The Fano Factor calculated at BF did not significantly differ between neurons in the three FRA classes (single- and double-peaked: $t = 0.70$, $p = 0.48$; single-peaked and complex: $t = 0.016$, $p = 0.99$), indicating that responses at BF were equally reliable for neurons with single- and multi-peaked FRAs (Figure 2E).

If single-peaked neurons have higher firing rates than those with more complex FRAs, any sampling bias toward more active neurons in extracellular recordings could make the spatial distribution of BF appear more homogeneous in electrophysiological mapping studies than in those using two-photon calcium imaging. To investigate this possibility, we used high channel count microelectrodes to isolate the tone responses of single neurons in layers 2/3 of ferret A1 (Figure 2-figure supplement 2;

see *Methods*), and the recorded FRAs were classified in the same way. The anesthetic regime, surgery, and stimuli were similar to our imaging experiments. Although all three FRA classes were observed, the microelectrode recordings yielded a higher proportion of neurons with single-peaked FRAs (Likelihood Ratio Test; $\chi^2 = 68.4457$, $p = 1.11 \times 10^{-16}$) than the imaging experiments, and fewer with double-peaked ($\chi^2 = 22.16$, $p = 2.50 \times 10^{-06}$) and complex ($\chi^2 = 30.06$, $p = 4.20 \times 10^{-08}$) FRAs (Figure 2F).

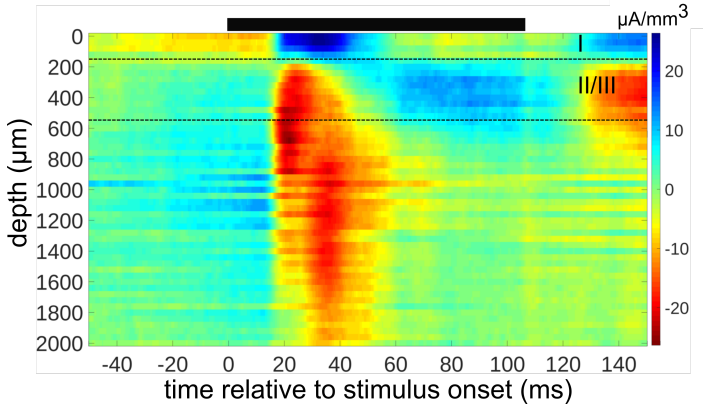

Figure 2-figure supplement 2. Determining cortical layers from a Current Source Density (CSD) map of electrophysiological responses. The CSD was constructed from local field potential recordings of responses to tones presented near BF (± 1/3 octave) in one microelectrode penetration. The black bar above the plot indicates stimulus presentation time. The depth in μm relative to the cortical surface is plotted on the y-axis. The boundary between layers 1 and 2 (upper black dotted line) was inferred based on the reversal from a source to a sink in the CSD profile, and the boundary between layers 3 and 4 (lower black dotted line) was estimated to be 400 μm below the beginning of layer 2.

Contrary to our two-photon imaging results, we did not find a significant difference between the spike rates of neurons with single- and double-peaked FRAs (t-test; $t = 1.29$, $p = 0.20$) or between those with single-peaked and complex FRAs ($t = 0.05$, $p = 0.96$) (Figure 2-figure supplement 3). This may result from a bias towards the most strongly responsive multipeaked neurons, given the small number of double-peaked and complex neurons measured using microelectrodes. Together, our results suggest that biases towards sampling single-peaked neurons in microelectrode recording studies could lead to estimates of more ordered tonotopy than two-photon calcium imaging in the same cortical region.

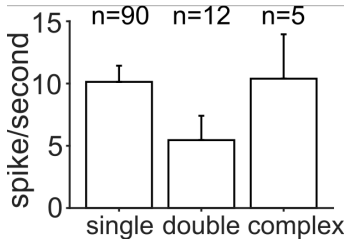

Figure 2-figure supplement 3. Magnitude of the trial-averaged response at BF, calculated from spike rates measured with microelectrodes. Responses were averaged across all neurons in each FRA class, pooled across penetrations and ferrets (mean ± SEM). The number of neurons per group is given above each bar.

The FRAs of single-peaked neurons can be well approximated by their BF. However, this is not the case for neurons with double-peaked and, in particular, complex FRAs. Consequently, an analysis based on BFs alone may be blind to an underlying organization of neurons with complex frequency receptive fields. To take into account a more complete representation of FRAs, we computed pairwise signal correlations. Correlations were calculated between pairs of frequency-sensitive neurons imaged simultaneously and belonging to the same FRA category: single-peaked, double-peaked and complex (Figure 3A), and were found to differ across the three classes (1-way ANOVA; $F = 389.7$, $p = 1.56 \times 10^{-163}$). In *post hoc* pairwise tests (Tukey's HSD), signal correlations within complex neurons (0.048 ± 0.003; mean ± SEM) were significantly lower than those for single-peaked (0.207 ± 0.002; $p = 9.561 \times 10^{-10}$) and double-peaked neurons (0.193 ± 0.002; $p = 9.561 \times 10^{-10}$). Similarly, signal correlations were significantly higher within single-peaked neurons than double-peaked neurons ($p = 4.43 \times 10^{-5}$). Furthermore, signal correlations decreased with cortical distance between neurons for single-peaked (Pearson's correlation; $r = 0.21$, $p = 5.29 \times 10^{-29}$; Figure 3E) and double-peaked cells ($r = 0.17$, $p = 1.48 \times 10^{-9}$; Figure 3F), but not for complex neurons ($r = 0.06$; $p = 0.12$; Figure 3G). These results further confirm that there is a greater degree of tonotopy for cells with simpler FRAs within a local cortical region.

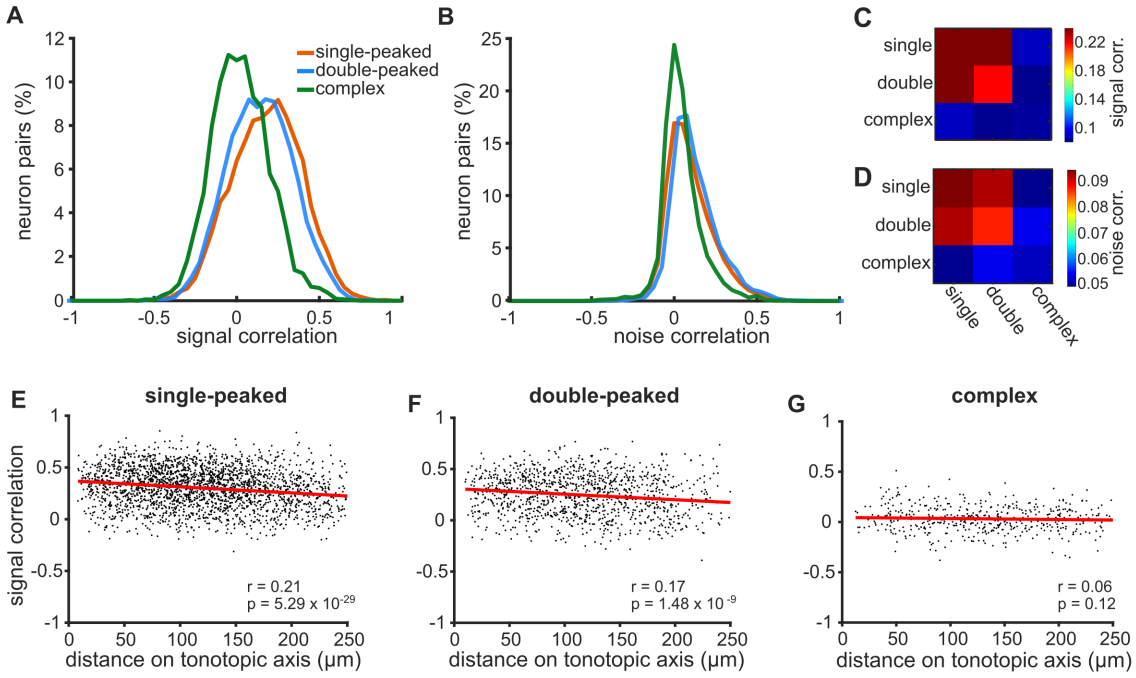

Figure 3. Correlations in neural activity are weaker and less spatially ordered for neurons with more complex FRAs. (A) Distributions of signal correlations in the pure tone responses of pairs of simultaneously imaged neurons with single-peaked (orange), double-peaked (blue) or complex (green) FRAs. **(B)** Distributions of noise correlations for the same neural pairs shown in **(A). (C)** The colour scale (right) shows the average signal correlation for pairs of neurons across all 9 combinations of the three FRA classes. **(D)** Noise correlations across FRA classes, presented as in **(C)**. **(E)** Pairwise signal correlations for single-peaked neurons plotted as a function of the distance between the two neurons along the tonotopic axis. The best linear fit to the data is shown (red line), with Pearson's correlation coefficient (r) and p-value (p) in the bottom right of the plot. **(F)** Same as **(E)**, but for double-peaked neurons. **(G)** Same as in **(E)**, but for complex neurons.

To investigate whether single- and double-peaked neurons share different local networks from those with complex FRAs, we calculated pairwise noise correlations, which are thought to reflect connectivity and common inputs between neurons[38] (Figure 3B). Indeed, the strength of noise correlations differed across the three FRA classes (1-way ANOVA; $F = 109.5$, $p = 9.405 \times 10^{-48}$). Noise correlations were significantly higher for single-peaked (0.122 ± 0.001; mean ± SEM) and double-peaked (0.124 ± 0.002) neurons than those with complex FRAs (0.071 ± 0.002; Tukey's HSD tests; single vs complex: $p = 9.561 \times 10^{-10}$; double vs complex: $p = 9.56 \times 10^{-10}$). Noise correlations did not differ between single-peaked and double-peaked neurons ($p = 0.86$). For all FRA types, noise correlations significantly decreased for pairs of neurons that were located further apart within the imaging field (Figure 3-figure supplement 1A-C).

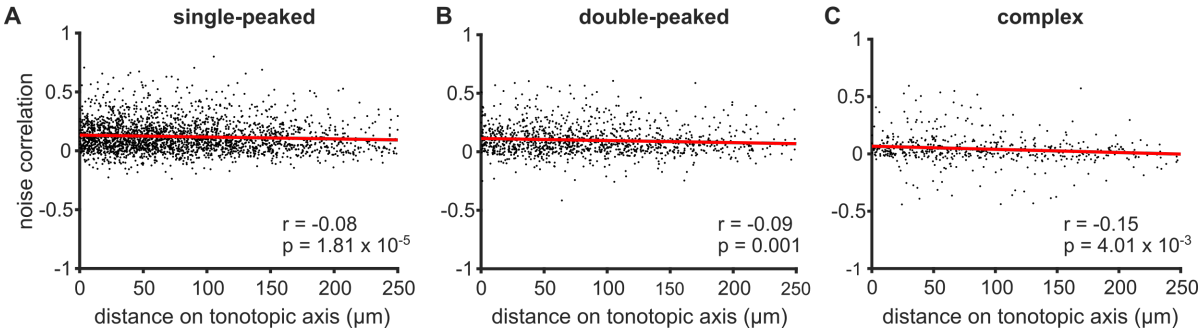

Figure 3-figure supplement 1. Noise correlations in neurons with single-peaked, double-peaked and complex FRAs. (A) Noise correlations for pairs of single-peaked neurons imaged simultaneously, as a function of the distance between the two neurons along the tonotopic axis. **(B)** Same as (**A**) for double-peaked neurons. **(C)** Same as **(A)** for complex neurons. Red lines indicate the best linear fit to the data. Pearson's correlation coefficient (r) and p-value (p) are also shown.

When we examined the correlation structure between neurons with different FRA classifications, we found that single- and double-peaked neurons had higher signal and noise correlations with one another than with complex FRA neurons (Figure 3C,D). This suggests that neurons with complex FRAs may differ in their connectivity within the local cortical network from those with simpler frequency tuning.

Frequency response organization at the global scale

To investigate tonotopic organization along the entire extent of ferret primary auditory cortex, all neurons imaged in our 8 ferrets were projected onto a common template of A1. These projections were aligned based on both an anatomical criterion (i.e. the gross anatomy of the ectosylvian gyrus), and a functional one (i.e. A1 boundaries derived from neuronal responses to tones) (Figure 4-figure supplement 1A,B; see *Methods*).

When single-peaked neurons were projected onto this global A1 template, the expected tonotopic gradient was clearly evident (Figure 4A1), with high frequencies mapped onto the dorsal tip of the ectosylvian gyrus (Figure 4B1) and lower frequencies toward the ventral border with secondary posterior fields[4,8]. The large-scale spatial organization of frequency preferences along the tonotopic

gradient was quantified as a correlation between BF_s and the neuron's position along the tonotopic axis (Pearson's correlation; r = -0.40, p = 1.1 x 10^{-12}; Figure 4C1).

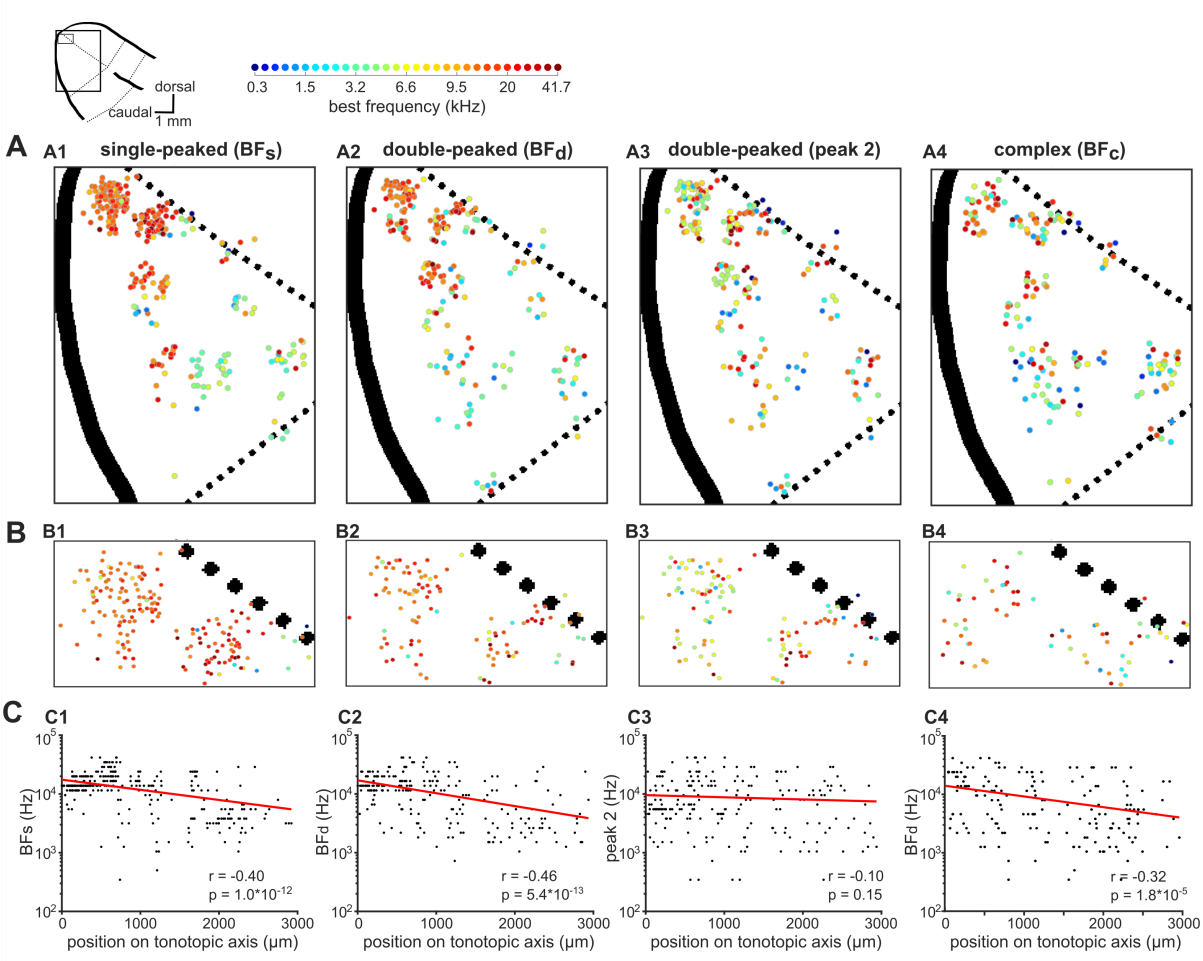

Figure 4. Global tonotopic organization of frequency preferences in ferret A1. The anatomical locations of neurons imaged across eight ferrets were projected onto a template map of auditory cortex, shown in the top-left corner. Thick black solid lines indicate sulci and black dotted lines indicate approximate borders between known cortical fields The two boxes represent the location of A1 (large box; **A**) and the most dorsal region of A1 (small box; **B**). **(A)** The BFs of individual neurons are color coded (legend above) and mapped onto A1. The spatial distributions of BF_s (**A1**), BF_d (**A2**), peak 2 of double-peaked neurons (**A3**), and BF_c (**A4**) are plotted separately. **(B)** Frequency preferences are mapped as in **(A)** for the dorsal tip of A1, where many neurons are occluded in **(A)**. **(C)** BF_s (**C1**), BF_d (**C2**), peak 2 (**C3**), and BF_c (**C4**) of each neuron are plotted against the neuron's position along the tonotopic axis on the template A1. Red lines show the best single-term exponential fits to the data, and Spearman's correlations (r) with their p-values (p) are also shown.

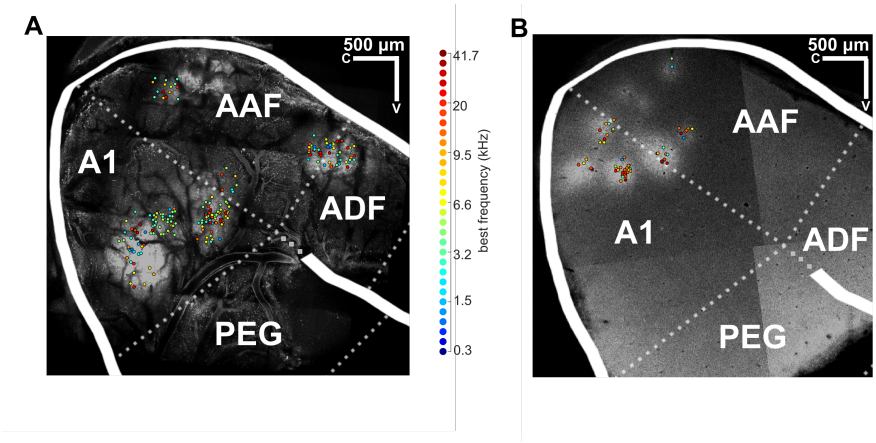

Figure 4-figure supplement 1. Mapping data from individual ferrets onto a common template of auditory cortex. (A) An image of the brain surface of ferret 3, acquired *in vivo* using two-photon calcium imaging (grey scale). Individual frequency-sensitive neurons imaged across all fields are plotted on this map according to their anatomical position, where their color indicates their BF (color scale right). The common template of auditory cortex is superimposed, where white solid lines indicate sulci and white dotted lines indicate approximate borders between known cortical fields (names in white text). The brain image and template were aligned according to the positions of sulci, and frequency responses of imaged neurons. Only neurons in A1 were included in our analyses. **(B)** A *post mortem* section of the auditory cortex of ferret 7, which was sliced parallel to the two-photon imaging plane (i.e. parallel to the surface of auditory cortex) and imaged with a confocal microscope. The BF of imaged neurons and the cortical template are superimposed, as in **(A)**. A1 = primary auditory cortex; AAF = anterior auditory field; PEG = posterior ectosylvian gyrus (containing the posterior pseudosylvian and posterior suprasylvian fields); ADF = anterior dorsal field.

When examining only neurons with double-peaked FRAs (BF_d), global tonotopy was clearly visible (Figure 4A2, B2), and this tonotopic gradient was again statistically significant ($r = 0.46$, $p = 5.7 \times 10^{-13}$; Figure 4C2). However, the BFs of double-peaked neurons varied more around their fitted tonotopic gradient (red line, Figure 4C2) than those of single-peaked neurons (t-test; $t = 2.43$, $p = 0.02$), suggesting that neurons with double-peaked FRAs have a less smooth tonotopic organization.

The BFs of neurons with complex FRAs were also organized tonotopically on the global A1 template ($r = 0.32$, $p = 1.82 \times 10^{-5}$; Figure 4A4, B4), but were more variable around the tonotopic gradient (Figure 4C4) than the BFs of either single-peaked ($t = 6.83$, $p = 2.68 \times 10^{-11}$) or double-peaked ($t = 4.50$, $p = 8.15 \times 10^{-6}$) neurons.

In contrast to BF, other aspects of the neurons' frequency responses were not found to be systematically ordered along the tonotopic gradient. The frequency of the second-strongest peak of double-peaked FRAs (peak 2) did not change systematically along this axis (r = -0.096, p = 0.15; Figure 4A3,B3,C3), nor did the differences between the two peaks of double-peaked neurons (r = 0.13, p = 0.054; Figure 4-figure supplement 2A-C).

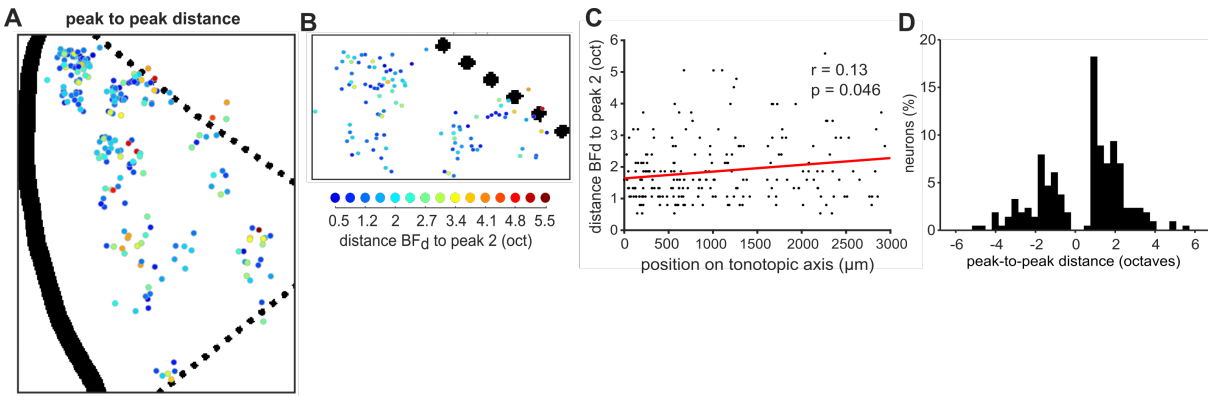

Figure 4-figure supplement 2. Mapping the peak-to-peak distances in double-peaked neurons. (A), (B) Double-peaked neurons imaged across all ferrets are mapped onto the template A1, as in Figures **4A** and **4B**. Here, the color scale (below **B**) indicates the difference, in octaves, between BF_d (i.e. the frequency eliciting the strongest response) and peak 2 (i.e. the frequency eliciting the second-strongest response) for each neuron. **(C)** The octave difference between BF_d and peak 2 is plotted for each double-peaked neuron, as a function of its position along the tonotopic axis (as in **Figure 4C**). The red line represents the best linear fit to the data, and the coefficient (r) and p-value (p) of Pearson's correlation are shown. **(D)** Distribution of the difference (in octaves) between BF_d and peak 2, across all double-peaked neurons. BF_d and peak 2 were on average 1.74 ± 0.07 (mean ± SEM) octaves apart, and their octave distances did not differ when BF_d was lower or higher than peak 2 (t-test, t = -0.17, p = 0.87).

These results indicate that, in ferrets, the BFs of A1 neurons are tonotopically organized at the global scale, but neurons with increasingly complex FRAs show more variance along the global tonotopic axis. Our analysis of both the local and global organization of frequency responses was carried out after removing the neuropil signal from each individual neuronal body. This procedure was necessary, as neuropil contamination can change the BF of individual neurons, particularly for those with complex frequency responses (see *Methods*; Figure 4-figure supplement 3A,B). For example, we found that neuropil signal introduced the appearance of a tonotopic order to an otherwise spatially disorganized signal – namely, the distance between the two peaks of double-peaked neurons (Figure 4-figure supplement 3D3).

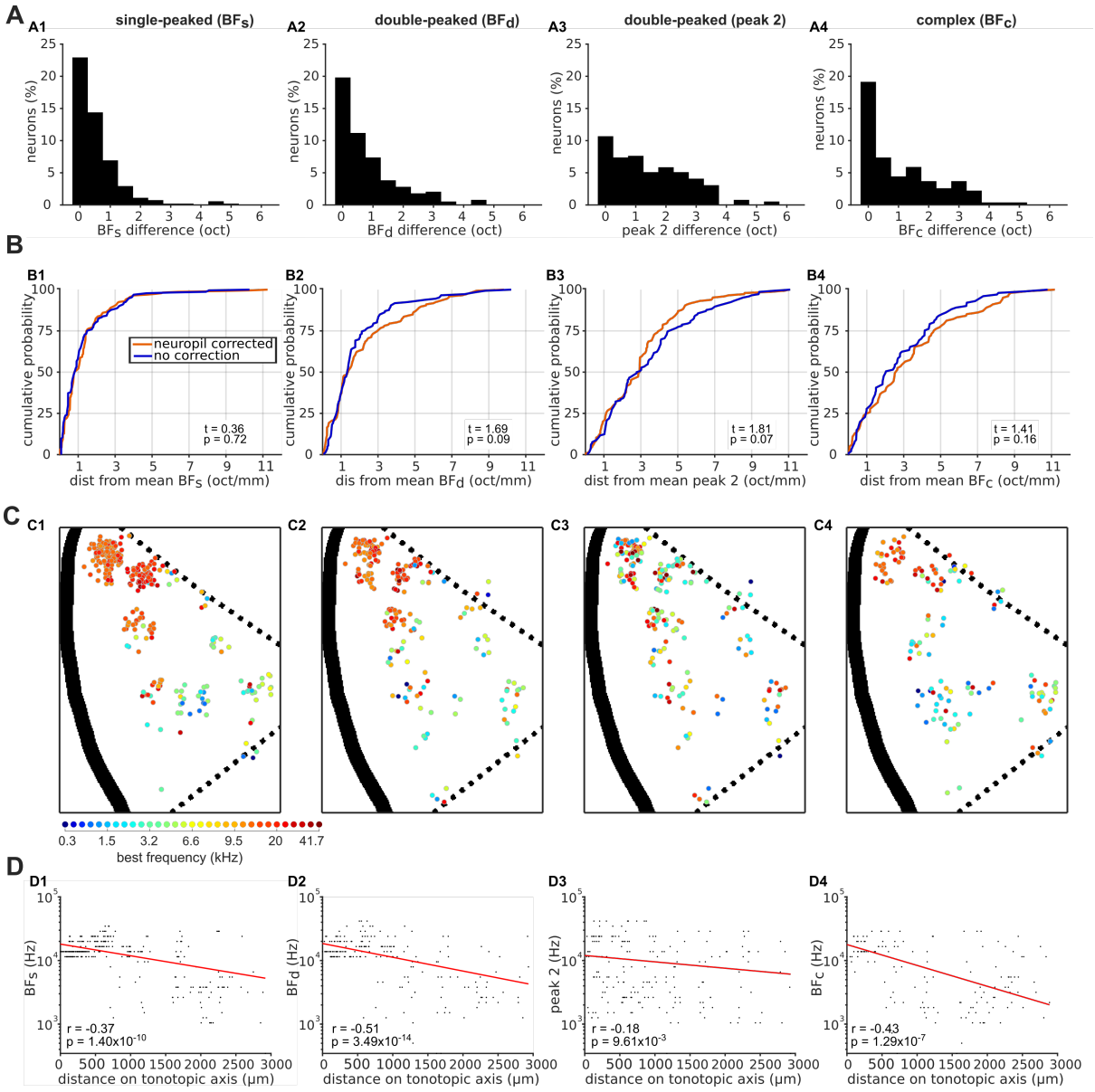

Figure 4-figure supplement 3. Effects of neuropil contamination on local and global tonotopic organization. (A) Distributions of the difference (in octaves) between BF_s (**A1**), BF_d (**A2**), peak 2 (**A3**) and BF_c (**A4**) calculated with and without neuropil signal subtraction. **(B)** Cumulative probability plots of the difference (in octaves) between each neuron's BF and the average BF of all frequency sensitive neurons in the same imaging field. Distributions for BFs obtained with (red) and without (blue) neuropil correction are plotted separately. The results of t-tests between the two distributions are given in the bottom right of each plot. **(C)** Frequency preferences are mapped onto a template A1, as in Figure **4A**, but here without neuropil correction. **(D)** Scatterplots show the frequency preferences of neurons as a function of their position along the tonotopic axis of the maps in **C** (as in Figure **4C**), for neuropil-uncorrected data.

Comparison of tonotopic organization in ferrets and mice

The contrast between local heterogeneity and global tonotopic organization of BFs, sometimes referred as "fractured" or "salt and pepper" organization, has been previously reported in the primary

auditory cortex of the mouse[16,17,19]. The results above show that a qualitatively similar organization exists in the ferret A1, but that much of the heterogeneity at both the local and global scales arises from neurons with complex frequency receptive fields. To directly compare the local organization of frequency preferences between mice and ferrets, we imaged neuronal responses in the primary auditory cortex of 11 mice under the same experimental conditions.

The BFs of neurons and their spatial organization within an example imaging field in the mouse are shown in Figures 5A and 5B, respectively. In keeping with previous studies[16,17], these plots suggest that the spatial organization of BFs in the mouse primary auditory cortex is also locally heterogeneous. Across all imaging fields, 854 of 1964 (43.75%) neurons were frequency-sensitive in mice (two-way ANOVA; $p < 0.05$), while only 693 of 3604 (19.23%) neurons were frequency-sensitive using the same statistical criterion in ferrets. Classification of neurons based on their FRAs confirmed that single-peaked, double-peaked, and complex neurons also exist in the mouse (Figure 5B), as they do in the ferret (Figure 2B). However, the relative proportions of these three FRA classes differ between the two species (Figure 5C). Specifically, a higher percentage of frequency-sensitive neurons in the mouse (60.54%) showed "simpler" frequency receptive fields with a single peak at BF, than in the ferret (42.71%; Likelihood Ratio Test, $\chi^2 = 48.96$, $p = 2.6 \times 10^{-12}$). Conversely, ferrets had more double-peaked (31.75% vs 26.23%; $\chi^2 = 5.67$, $p = 0.017$) and complex FRAs (24.96% vs. 13.23%; $\chi^2 = 34.83$, $p = 3.60 \times 10^{-9}$) than mice. This suggests that frequency receptive fields in the superficial layers of ferret A1 may be more complex overall than those in mice.

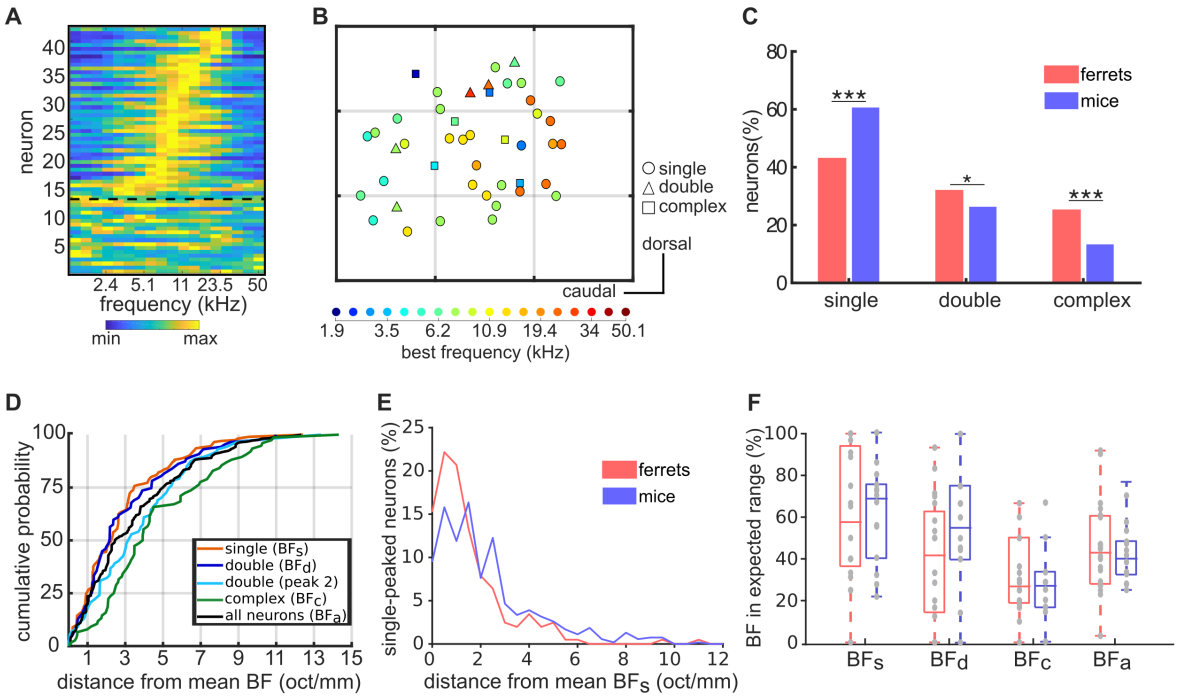

Figure 5. Similar tonotopic organization in the primary auditory cortex of ferrets and mice. **(A)** Frequency Response Profile of all neurons imaged in one imaging field in one mouse. Data are presented as in Figure **1C**. **(B)** Map of the anatomical locations of the neurons in **(A)**, plotted as in Figure **2B**. Neurons are color-coded according to their BF, and their shape corresponds to their FRA class. Each grey grid corresponds to a cortical area of 100 x 100 µm. **(C)** Proportion of frequency-sensitive neurons from each FRA class for ferrets (red) and mice (blue). The results of Likelihood Ratio tests are indicated above (*p < 0.05 and *** p < 0.001). **(D)** Cumulative probability plots of the difference (octaves/mm) between the BF of each neuron and the average BF of all neurons in the same imaging field. As in Figure **2C**, distributions were calculated separately for BF_s (orange), BF_d (dark blue), peak 2 of double-peaked neurons (light blue), BF_c (green), and BF_a (black). **(E),** Distributions of the distance in octaves per mm between the BF_s of each single-peaked neuron in an imaging field and the average BF of these neurons. Data are shown for ferrets (red) and mice (blue). **(F)** Box plots showing the percentage of neurons having a BF within the expected frequency range, given the species, size and average BF of each imaging field. Percentages were calculated separately for BF_s, BF_d, BF_c and BF_a, and percentages for individual imaging fields are shown as grey dots. Boxplots for ferrets (red) and mice (blue) show the median, upper quartile, and lower quartile of each dataset.

Could the presence of double-peaked and complex FRAs help explain the local variance in cortical tonotopy in mice, as we observed in ferrets? To answer this question, the BF variance within an imaging field was calculated separately for single-peaked, double-peaked and complex neurons (Figure 5D), in every imaging field containing at least three neurons of each FRA class. Unlike in ferrets, the BF variability of double-peaked neurons (3.31 ± 0.18 oct/mm; mean ± SEM) was not significantly higher than that of single-peaked neurons (2.70 ± 0.12 oct/mm; t-test; t = -0.68, p =0.50) in mice, and the BF variability of the two peaks of double-peaked neurons did not differ significantly

304 ($t = 1.91$, $p = 0.059$). In line with our ferret data, however, the BFs of neurons with complex FRAs
305 (4.62 ± 0.34 oct/mm) were more variable than those of single-peaked ($t = 5.34$, $p = 1.9 \times 10^{-7}$) and
306 double-peaked ($t = 3.73$, $p = 0.0020$) neurons, suggesting that the frequency preferences of neurons
307 with more complex FRAs are less tonotopically organized within the local microcircuit.
308
309 Directly comparing the degree of local organization of frequency preferences between ferrets and
310 mice is not as straightforward as it might initially seem. The A1 tonotopic gradient is shorter in the
311 mouse (~1 mm)[14,15] than the ferret (~3.5 mm)[4,8], and the audible hearing range is 2-60 kHz in
312 C57BL/6 mice[39,40] and 0.3-44 kHz in ferrets[41]. Comparisons of tonotopic maps between these two
313 species must take these anatomical and hearing range differences into consideration. To illustrate this
314 point, Figure 5E compares histograms of the BF_s variance in ferrets and mice, expressed in units of
315 octaves per mm. The BFs of single-peaked neurons were more variable within a millimetre of A1 in
316 mice (2.25 ± 0.09 octave/mm) than in ferrets (1.50 ± 0.11; t-test; $t = 4.73$, $p = 2.68 \times 10^{-6}$). This may
317 be taken to suggest that BF_s is more locally variable in mouse primary auditory cortex than in ferrets,
318 but this metric does not account for the species differences in hearing range and tonotopic axis length.
319
320 To account for this difference, we computed the percentage of neurons that had a BF within the
321 expected frequency range in each species, for a given imaging field. The expected BF range was
322 calculated based on the diameter of the imaging field, the average BF across all neurons in the field,
323 and an expected tonotopic gradient of 4.91 oct/mm in mice and 2.93 oct/mm in ferrets. The
324 percentage of neurons with a BF within the expected range provided a measure of the variance in
325 tonotopic organization that could be directly compared between species, and was computed separately
326 for neurons with: 1) single-peaked FRAs; 2) double-peaked FRAs; 3) complex FRAs; and 4) all three
327 FRA types combined (Figure 5F). The resulting values varied across the three different FRA classes
328 (two-way ANOVA; $F = 9.80$, $p = 7.22 \times 10^{-6}$), but did not differ between mice and ferrets ($F = 0.68$, p
329 $= 0.41$), and there was no evidence of an interaction between species and FRA type ($F = 0.96$, $p =$
330 0.41). In *post hoc* pairwise tests, the proportion of BFs within the expected range did not differ
331 between mice and ferrets for any of the FRA classes examined (Tukey's HSD tests; $p > 0.05$).

Taken together, these results suggest that mice and ferrets have comparable local heterogeneity in frequency preferences within well-tuned (i.e. single-peaked or double-peaked) neurons in layers 2/3 of primary auditory cortex. More complex frequency tuning is associated with more variance in the frequency preferences of neighboring neurons in both species.

Discussion

We used two-photon calcium imaging to study the representation of sound frequency in populations of neighboring neurons in mouse and ferret primary auditory cortex. Previous studies in mice have described global A1 tonotopy with local variability of frequency preferences[16,17,19], and here we show that ferret A1 shares the same spatial organization. Furthermore, we demonstrate that the complexity of frequency receptive fields can account for much of the local heterogeneity in both mice and ferrets. Thus, the fractured sensory maps described in primary cortical areas may be a consequence of complex stimulus feature extraction.

Primary auditory cortex is tonotopically organized at the global scale

Electrophysiological and widefield imaging studies have described a tonotopic gradient in the primary auditory cortex of all mammalian species studied, including humans[42], monkeys[2], cats[3], ferrets[4], gerbils[5], rats[6] and mice[15]. This global tonotopic organization has been confirmed in two-photon calcium imaging studies of primary auditory cortex in mice[16–18] and marmosets[31]. Here, we performed the first two-photon calcium imaging of auditory cortex in carnivores, and show that this result generalizes to ferrets. The stereotyped position of ferret A1 within reliable anatomical landmarks allowed us to combine data from multiple animals onto a template of A1, as in previous electrophysiological studies[43]. This map showed a clear dorsal-to-ventral tonotopic gradient for neurons with single-peaked, double-peaked and, to a lesser extent, complex frequency receptive fields. In contrast, we observed no systematic spatial arrangement of the second frequency peak, or the difference between frequency peaks in double-peaked neurons. Together, these findings support

the well-established idea that global tonotopy is the main spatial organizational principle in primary auditory cortex, and is observed within all neurons that are frequency sensitive.

Tonotopy is well preserved locally for neurons with simple, but not complex, frequency receptive fields

An advantage of two-photon calcium imaging over other techniques is its ability to sample the activity of large numbers of individual neurons within a local cortical region, while knowing their relative spatial locations. In both ferrets and mice, neurons with single-peaked FRAs were organized homogeneously, with almost 90% of them in a given imaging field presenting BFs within the expected frequency range, assuming a tonotopic gradient of <2.9 oct/mm in mice and 4.9 oct/mm in ferrets. Signal correlation analyses further confirmed local tonotopic organization, as proximate neurons were more similarly tuned than distant ones within an imaging field (~250 μm^2). Double peaked neurons were less ordered, with ~60% of their BFs within the expected range and greater local variability around the global tonotopic gradient, compared to single-peaked neurons. The BFs of neurons with complex frequency responses were even more spatially varied than double-peaked neurons. In contrast to single- and double-peaked neurons, only 30% of complex neurons in a given imaging field were within the expected BF range, and their signal correlations were lower and less spatially dependent. Romero et al. have recently shown that BFs are more locally variable among neurons with less well-defined frequency tuning[20]. Here, we further show that BFs are also more variable among nearby neurons with complex frequency receptive fields, even when their trial-to-trial responses at BF are equally reliable (as shown by our Fano Factor analyses). The association between frequency receptive field complexity and tonotopy was remarkably similar for mice and ferrets, suggesting that this may be a common feature of the mammalian cortex. The complexity of receptive fields may also explain the observed local variability of orientation tuning in V1[23,44] and whisker preferences in barrel cortex[21,22].

The departure from strict tonotopy in A1, compared to earlier processing stations, such as the central nucleus of the inferior colliculus[45], may in fact be an unavoidable result of complex spectrotemporal

processing. We found that noise correlations were lower within local populations of complex neurons than within single- and double-peaked neurons. This may be due to neurons with complex frequency responses making more horizontal connections with distant cortical columns, or receiving inputs from layer 4 neurons in different areas of the tonotopic map. In V1, synaptic connections are more probable among V1 neurons with similar orientation tuning[46]. From our experiments, we might expect A1 neurons with simple frequency tuning to have stronger local connections to similarly tuned neurons, supporting well-defined tonotopy. Those with complex frequency responses, on the other hand, may receive inputs from neurons in more distant regions of the tonotopic gradient.

Similarities and differences between mice and ferrets

Our results show that an equivalent tonotopic organization of well-tuned neurons exists in ferrets and mice, despite the fact that the A1 of ferrets represents ~3 oct/mm, while that of mice represents ~5 oct/mm. Thus, local heterogeneity in the tonotopic map is unlikely to be due to limitations in brain size, or other potential factors that are inherent to rodents.

In contrast to this view, Zeng et al.[31] recently reported that BFs of A1 neurons are more locally variable in rats than in marmosets. It is possible that the marmoset cortex contains a smoother tonotopic arrangement than other species studied, and this would be consistent with the high number of single-peaked neurons presented in their study[31]. Alternatively, the reported difference between marmoset and rat A1 tonotopy might be accounted for if differences in the size of A1, complexity of frequency tuning, and hearing ranges of these two species are taken into consideration.

Issa et al.[18] reported more homogenous tonotopy in mouse A1 than other two-photon imaging studies[16,17,19,20,26], although the local variability in BF was still higher than that of marmosets[31]. Two distinguishing methodological features of Zeng et al.[31] and Issa et al.[18] are: (1) Issa et al. imaged tone responses in awake animals, and (2) neither study applied neuropil corrections. Both two-photon calcium imaging[20,26] and single unit electrophysiological studies[14] have demonstrated that there is little change in a neuron's BF between passively listening and anaesthetized states, so this alone is

unlikely to account for the smooth tonotopy observed by Issa et. al.[18]. Neuropil signals contaminating neural responses can lead to smoother tonotopic maps[20], on the other hand, as the signals in axons and dendrites are averaged across the local population. In fact, our comparison of data with and without neuropil correction (Figure 4-figure supplement 3) demonstrated that neuropil contamination can result in the second, weaker peak of double-peaked neurons appearing to be tonotopically organized, while this is not spatially ordered in the neuropil-corrected signal.

Our study highlighted two main differences between mice and ferrets. First, in both species, the majority of neurons were not sensitive to changes in tone frequency, but fewer A1 neurons exhibited frequency sensitivity in ferrets (19%) than in mice (44%). While these numbers may seem low, most A1 neurons do not even respond to pure tones[19,26]. Therefore, it is important to keep in mind that tonotopic maps do not reflect the spatial organization of response properties of most auditory cortical neurons. Second, a greater proportion of frequency-sensitive neurons showed double-peaked or complex FRAs in ferrets than in mice. In contrast, the proportions of multi-peaked neurons in our microelectrode recordings in ferret A1 are equivalent to those reported in marmoset A1 recordings[36].These results may indicate that neurons in ferret and marmoset A1 are better suited to integrate information across frequency bands or encode more complex spectrotemporal features. For example, neurons with multiple frequency peaks would be useful for identifying sound sources based on their spectral timbre[43], or may provide harmonic templates for pitch perception[47]. Further physiological and behavioural studies are required to test these potential species differences in auditory cortical function.

Comparison to previous electrophysiological studies

With some exceptions[8], electrophysiological studies have typically reported smoother tonotopic gradients than two-photon imaging studies[13,15]. Our results offer an explanation for this inconsistency across methodologies. Compared to neurons with more complex FRAs, the BFs of single-peaked neurons are more precisely mapped at both the local and global scale, and they also have stronger responses, as measured through their calcium dynamics (Figure 2D). Because extracellular

444 microelectrode recordings are more likely to detect and cluster neurons with higher firing rates[48], such
445 studies may oversample neurons with single-peaked FRAs and therefore with more precise tonotopy.
446 In support of this hypothesis, we found that >80% of frequency-sensitive neurons that we recorded
447 from superficial A1 using microelectrodes had single-peaked FRAs - approximately double the
448 proportion of single-peaked FRAs identified using two-photon calcium imaging in the same species.
449 An electrophysiological study of marmoset auditory cortex also found that 20% of neurons showed
450 multi-peaked frequency tuning[36].
451
452 Electrophysiological studies in mice have also reported that the granular layers of A1 are more
453 tonotopically ordered than supragranular layers[13–15]. However, two-photon imaging studies have
454 provided conflicting evidence about this[25,26]. We suggest that the more ordered tonotopy in layers 4/5
455 may arise from a larger proportion of single-peaked neurons in this part of the cortex. This is
456 consistent with the electrophysiological data of Guo et al.[14], who report that more neurons with
457 unreliable frequency tuning exist in the superficial layers of mouse A1. Here, we show that tonotopic
458 variability in layers 2/3 is not simply due to neurons having less reliable responses, but is also
459 associated with neurons that respond to a combination of distinct frequency bands.
460
461 *Conclusions*
462 Applying two-photon imaging to the study of neuronal activity in the ferret auditory cortex for the
463 first time, we found that A1 neurons tuned to a single best frequency are tonotopically organized at
464 both the local and the global scales. The presence of neurons with more complex FRAs fractures this
465 tonotopic order, increasing the local heterogeneity of neuronal frequency preferences, just as it does in
466 mice. Cells with complex sensory receptive fields are likely to be important for extracting information
467 from natural environments, and are more common in ferrets than mice. Future imaging studies are
468 required to better understand the functional properties and connectivity of these subpopulations of
469 neurons.
470
471

Methods

Animals

All animal procedures were approved by the local ethical review committee of the University of Oxford and performed under license from the UK Home Office. Eight female ferrets (*Mustela putorius furo*; Marshall BioResources, UK) and 11 female mice (C57BL/6J; Harlan Laboratories, UK) were used in the two-photon imaging experiments, and six ferrets (two male) were used in the electrophysiology experiments.

Viral vector injections

Ferret surgery

At age 8–12 weeks, ferrets were put under general anesthesia with an intramuscular injection of ketamine (Vetalar; 5 mg/kg) and medetomidine (Domitor; 0.02 mg/kg), and medicated with buprenorphine (Vetergesic; 0.02 mg/kg i.m.), atropine (Atrocare; 0.06 mg/kg i.m.) and meloxicam (Metacam; 0.2 mg/kg i.m.). Ferrets were then intubated and artificially ventilated. A mixture of oxygen and isoflurane (IsoFlo; 0.5 – 2%) was continuously delivered throughout the surgery to maintain anesthesia. Respiratory rate, end-tidal CO_2, electrocardiogram, blood pressure, and blood oxygenation were continuously monitored, and body temperature was maintained at 36-38°C (3M™ Bair Hugger™). The eyes were lubricated (Maxitrol, Alcon) to prevent corneal desiccation. An intravenous cannula was inserted to deliver Hartmann's solution (54ml/kg/hr) continuously, a single dose of co-amoxiclav (Augmentin, 20mg/kg), and medetomidine (Domitor; 0.027 mg/kg i.m.) as required, throughout the surgery. After placing the ferrets in a stereotaxic frame (Model 900LS, David Kopf Instruments), the scalp was cleaned (ChloraPrep®; 2% chlorhexidine gluconate), bupivacaine (Marcain; 2mg/kg, s.c.) was injected into the scalp, the scalp was incised, and the right temporal muscle was retracted. A craniotomy and durotomy were carried out to expose the primary and secondary auditory cortex, based on stereotaxic coordinates (11 mm ventral to the midline and 8 mm frontal to Lambda) and visual confirmation of the ectosylvian gyrus.

Injections were carried out using a glass pipette and a custom-made pressure injection system. The viral vector consisted of a 1:1 solution of AAV1.Syn.GCaMP6m.WPRE.SV40 (Penn Vector Core) and phosphate-buffered saline (PBS; Sigma Aldrich) for ferrets 1- 4, and a 1:1 solution of AAV1.Syn.GCaMP6f.WPRE.SV40 (Addgene) and AAV1.mDlx.GFP-GCaMP6f-Fishell-2.WPRE.SV40 (Penn Vector Core) for ferrets 5-8. Approximately 260 nl of the viral vector was slowly injected at depths of ~800, 600, 400 and 200 µm below the pial surface in ferrets 1-4 and at depths of 200 µm and 400 µm in ferrets 5-8. For each ferret, the viral vector solution was injected into 4 - 9 sites across primary and secondary auditory cortex.

The bone was then replaced over the craniotomy, the muscle, fascia and skin were sutured closed, and the animal was recovered. Dexamethasone (0.5 mg/kg i.m.) and buprenorphine (0.01 mg/kg i.m.) were administered immediately after surgery. Meloxicam (0.2 mg/kg oral) and co-amoxiclav (20 mg/kg s.c.) were administered daily for 5 days, and buprenorphine (0.01 mg/kg i.m.) for two days.

Mouse surgery

Mouse experiments were previously reported in Panniello et al.[19]. At age 5-6 weeks, mice were premedicated with dexamethasone (Dexadreson; 4 µg s.c.), atropine (Atrocare; 1 µg s.c.) and carprofen (Rimadyl; 0.15 µg s.c.), and put under general anesthesia with fentanyl (Sublimaze; 0.05 mg/kg i.p.), midazolam (Hypnovel; 5 mg/kg i.p.), and medetomidine hydrochloride (Domitor; 0.5 mg/kg i.p.). The mouse was then placed in a stereotaxic frame (Model 900LS, David Kopf Instruments) and maintained at 36-37°C body temperature throughout surgery (DC Temperature Controller, FHC). The scalp was incised, the temporal muscle retracted, and A1 was located using stereotaxic coordinates (70% of the distance from Bregma to Lambda, and ~4.5 mm lateral from the midline). Two small holes (~0.4 mm diameter), separated rostrocaudally by ~0.5 mm, were drilled over the right A1. A total of ~200 nl of the viral construct AAV1.Syn.GCaMP6m.WPRE.SV40 (Penn Vector Core), diluted (1:2) in PBS, was injected at each site, spread equally across four depths spanning 50-400 µm below the pial surface. After injection, the skin was sutured and general anesthesia was reversed with flumazenil (Anexate; 0.5 mg/kg s.c.) and atipamezol (Antisedan; 2.5

mg/kg s.c.). Postoperative buprenorphine (Vetergesic; 1 ml/kg s.c.) and enrofloxacine (Baytril; 2 ml/kg s.c.) were administered immediately after surgery and again 24 hours later.

In vivo two-photon calcium imaging

Ferret surgery

In vivo two-photon imaging was performed 3–6 weeks after viral injection. General anaesthesia was induced with an intramuscular injection of ketamine (Vetalar; 5 mg/kg) and medetomidine (Domitor; 0.02 mg/kg), and was maintained with a continuous intravenous infusion of these two drugs in Hartmann's solution with 3.5% glucose and dexamethasone (0.5 mg/ml/hr). The animal was intubated and artificially ventilated. Respiratory rate, end-tidal CO_2, electrocardiogram and blood oxygenation were continuously monitored throughout the imaging session. Eye ointment (Maxitrol; Alcon, UK) was applied throughout and body temperature was maintained at 36-38°C. Atropine (Atrocare; 0.06 mg/kg i.m.) was administered every 6 hours, or when bradycardia or arrhythmia was observed. Ferrets were placed in a custom-built stereotaxic frame and head stability was achieved using ear bars and a mouthpiece. After shaving the scalp and injecting bupivacaine (Marcain, 2mg/kg s.c.), the skin was incised and the temporal muscle removed. A steel holding bar was secured to the skull using dental cement (SuperBond; C&B, UK) and a stainless steel bone screw (Veterinary Instrumentation, UK). A circular craniotomy 10 mm in diameter was drilled over the injection site, and any dura that had regrown over the auditory cortex was removed. A custom made titanium ring (10 mm diameter) containing an 8 mm glass coverslip (Thermo Fisher Scientific, UK) was inserted in the craniotomy and secured to the skull with dental cement. Ear bars were removed, and the ferret was placed under the microscope for imaging.

Mouse surgery

In vivo two-photon imaging was performed 3–6 weeks after viral injection. All mice were imaged at <12 weeks of age, before the development of high frequency hearing loss[40] . General anaesthesia was induced with an intraperitoneal injection of ketamine (Vetalar; 100 mg/kg) and medetomidine (Domitor; 0.14 mg/kg), and was maintained with hourly subcutaneous injections of both agents (50

mg/kg/h Vetalar and 0.07 mg/kg/h Domitor). Body temperature was maintained at 37-38°C with a heating pad. The mouse was moved to a stereotaxic frame (Model 900LS, David Kopf Instruments), the scalp was incised, the temporal muscle retracted, and a craniotomy of ~2.5 mm diameter was performed over the injection sites in the right auditory cortex. The exposed area was covered with a glass coverslip, which was secured to the skull with cyanoacrylate adhesive (UltraGel; Pattex, DE). A steel holding post was attached to the left side of the skull using dental cement (UniFast Trad, GC Dental Products Corporation), ear bars were removed, and the mouse was placed under the microscope in the stereotaxic frame.

Two-photon imaging

Imaging of calcium transients was performed using a B-Scope two-photon microscope (Thorlabs, Inc., UK) controlled by ScanImage 4.1 software (http://scanimage.org). Excitation light was emitted by a Mai-Tai eHP laser (SpectraPhysics, UK; 70 fs pulse width, 80 MHz repetition rate) tuned to 930 nm. The beam was directed into a Conoptics modulator (laser power, as measured under the objective, was 15–30 mW) and scanned through an 8 kHz resonant scanner in the *x*-plane and a galvanometric scanning mirror in the y-plane. The resonant scanner was used in bidirectional mode, at a resolution of 512 × 512 pixels, allowing us to acquire frames at a rate of ~30 Hz for our most common zoom. A 16X/0.80W LWD immersion objective (Nikon, UK) was used, and emitted photons were guided through a 525/50 filter onto GaAsP photomultipliers (Hamamatsu Photonics, Japan). Neuronal fields were between 200 x 200 µm and 300 × 300 µm in size. Neuronal activity was imaged in ferrets at 176 ± 26.83 µm (median ± s.d.) below cortical surface. In mice, imaging was performed at 216 ± 34.21 µm below pial surface, corresponding to layer 2/3 in this species[49,50].

Sound presentation

Pure tones were generated via Matlab (MathWorks, Inc., USA), and an RZ6 multiprocessor (Tucker-Davis Technologies, USA) was used to synchronize the sound presentation with the microscope scanning.

Sound stimuli were presented binaurally to the animal via a customized closed acoustic delivery system comprised of either two Tucker-Davis Technologies EC1 electrostatic speakers (11 mice and three ferrets) or two Panasonic RPHV297 earphones (5 ferrets). Speakers were coupled to a 12-cm-long silicone tube leading into the ear canal. The output response of the speakers was measured using a Brüel & Kjær calibration system with a GRAS 40DP microphone coupled to the end of the silicone tube. An inverse filter was applied to the speaker output to produce a flat spectral response (±3 dB) over the tone frequency range. Sound intensity was calibrated with an Iso-Tech TES-1356-G sound level calibrator.

The microscope and experimental animals were enclosed within a sound- and light-attenuating box. The ambient room noise was <42 dB SPL inside this box, and primarily consisted of energy at <200 Hz. The resonant scanner generated a constant acoustical tone of 8 kHz during imaging that was <30 dB SPL near the animal's head.

For each imaging field in the ferret experiments, 10-20 repetitions of pure tones were presented at frequencies with 0.25 octave spacing across the ferret hearing range, and levels of 30-90 dB SPL, with 20 dB spacing (50 to 125 ms onset and offset cosine ramps). Frequency/level combinations were presented in pseudorandom order. Details of stimulus parameters for each animal are given in Table 1. For mice, ten repetitions of 100-ms duration (5 ms onset and offset cosine ramps) pure tones were presented at 18 frequencies (1.9–50 kHz, 0.6 octave spacing) and 4 levels (40, 60, 80, and 100 dB SPL), at a rate of 0.65 Hz.

ferret	stimulus duration (ms)	repetitions	interstimulus interval (s)	frequency range (Hz)
1	100	10	0.75	1259-41687
2	500	12	1.50	1047-28840
3	100	10	1.33	1259-41687
4	100	10	1.33	1259-41687
5	500	12	1.50	346-28840
6	500	20	1.50	346-28840
7	500	12	1.50	1047-28840
8	500	12	1.50	1047-28840

Table 1. Details of stimuli presented to ferrets

Histology

At the end of each imaging session, experimental animals were overdosed (mice: 100 mg/kg ketamine and 0.14 mg/kg medetomidine, i.p.; ferrets: Euthatal, 1 ml pentobarbital sodium, i.p.) and perfused transcardially, first with 0.01 M phosphate-buffered saline (PBS) and heparin (20 units/ml), and then with 4% paraformaldehyde in PBS. Brains were removed and placed in 4% paraformaldehyde for two hours, after which they were stored in PBS with 0.01% sodium azide. Ferret brains were then cryoprotected in a 1:3 solution of sucrose and PBS for 24 hours. Sagittal brain sections (50 µm thickness) were obtained using a freezing sliding microtome (Leitz Wetzlar). Sections were sliced parallel to the orientation of the *in vivo* cranial window to facilitate the reconstruction of imaged neurons. Sections were washed three times in PBS, after which they were mounted onto microscope slides using Vectashield mounting medium (Vector Laboratories Ltd., USA). A coverslip was placed on the slide for imaging and sealed with clear nail polish.

Confocal imaging

Brain sections were imaged using an inverted Olympus FV3000 six laser line spectral confocal microscope fitted with high sensitivity gallium arsenide phosphide (GaAsP detectors) and a 4x, 0.16 NA UplanSApo objective. The confocal pinhole was set to one airy unit to optimize optical sectioning with emission collection. Images were collected in resonant scanning mode at 512x512 pixels (pixel size 6.21µm) and 16x averaging. Tile scans were stitched using the Olympus FluoView software.

Identifying the location of GCaMP6 injection sites

A tracing of the ectosylvian and pseudosylvian sulci in ferret 7 was used as a template of auditory cortex, and imaging fields from all 8 ferrets were transferred onto this template. In ferrets 1, 5, 6 and 7, 1mm x 1mm images of the brain surface were acquired *in vivo* at the beginning of the two-photon imaging session, across the entire craniotomy. These images were then tiled together to reconstruct the surface of auditory cortex and locate the imaged fields. The tiled auditory cortex was then aligned

633 with boundaries of the sulci in the auditory cortical template (Supplementary Fig 6a). For ferrets 2, 3,
634 4 and 8, GCaMP6 injection sites viewed on confocal images of the ferret ectosylvian gyrus (above)
635 were aligned with the two-photon imaging fields acquired in the same ferret to precisely determine the
636 location of each imaged field on the gyrus. The confocal images were then aligned to the sulci in the
637 template map of the ectosylvian gyrus (Figure 4-figure supplement 1), using custom Matlab scripts.
638 These procedures allowed us to plot the coordinates of neurons imaged in different animals onto a
639 common map of auditory cortex.
640
641 **Data analysis for two-photon imaging experiments**
642 *Isolating the responses of single neurons from imaging fields*
643 We analysed the responses of 3604 neurons imaged in 32 imaging fields across 8 ferrets, and 1962
644 neurons imaged in 42 imaging fields across 11 mice.
645
646 Videos of the imaging field during tone presentation were imported into Suite2p software
647 (https://github.com/MouseLand/suite2p), which automatically performs mechanical drift correction,
648 cell detection, and neuronal and neuropil trace extraction, and spike deconvolution. Parameters for the
649 estimation of calcium transient templates were set separately for GCaMP6m and GCaMP6f, as the
650 rise and decay times differ for these two indicators. These parameters were optimized using our own
651 dataset. The most relevant parameter was the half decay time of the indicator (0.7 for GCaMP6f and
652 1.25 for GCaMP6m.
653
654 We manually inspected all regions of interest automatically detected by the Suite2p built-in classifier,
655 in order to confirm if they were individual healthy neurons. This assessment was based on the frame-
656 averaged image (e.g. the candidate neuron had a clear ring of florescence and was dark in the center),
657 the alignment of the region of interest (e.g. the region did not expand beyond the cell membrane or
658 include other neruons), and the activity of the calcium trace (e.g. no evidence of "bursting" that
659 characterizes cell death). For each confirmed neuron, time series of the neuronal calcium trace

660 ($\Delta F/F_0$), neuropil calcium trace, and deconvolved spike probability were exported to Matlab for
661 further analysis.
662
663 *Identifying frequency sensitive neurons*
664 Neuronal responses to sound presentation were quantified within a time window starting at stimulus
665 onset and lasting twice as long as the stimulus. The "evoked activity" was defined as the average of
666 the inferred spike probability trace within the response window. A two-way ANOVA, with tone
667 frequency and sound level as predictors, was used to determine if the evoked activity was
668 significantly modulated by sound frequency or intensity ($\alpha = 0.05$). Neurons showing a significant
669 main effect of frequency or frequency/level interaction were defined as "frequency sensitive", and
670 only these neurons were included in further analyses.
671
672 *Calculating best frequency and classifying the frequency response*
673 FRA plots were constructed for a given neuron from the trial-averaged evoked activity in response to
674 tones presented at each frequency/level combination. For visualization, FRA plots were smoothed
675 using a two dimensional three-point Gaussian kernel.
676
677 Frequency profiles of neurons were calculated by averaging the FRA across all sound levels. The
678 frequency eliciting the highest response in the frequency profiles was defined as the BF, as in
679 previous studies[14,19,45].
680
681 Neurons were automatically categorized into three classes based on their frequency-response profiles.
682 A neuron was defined as "single-peaked" if its frequency-response profile contained only one
683 continuous region above threshold, where threshold was defined as 75% of the maximal response
684 across all frequencies. "Double-peaked" neurons were those with two distinct regions above threshold
685 in their frequency-response profile. For these FRAs, the frequency eliciting the strongest response was
686 defined as $BF_{d,}$ while the frequency eliciting the highest response in the other response region was
687 defined as peak 2. A neuron was defined as "complex" if it showed more than two discontinuous

regions above threshold in the frequency-response profile. We also visually inspected FRAs (both smoothed and unsmoothed) of neurons and manually classified them as single-peaked, double-peaked or complex. The classification of 83% of neurons was the same under the automated frequency profile or manual FRA classification procedures. For the remaining 17% of neurons, the final classification was based on visual inspection of the FRA and frequency-response profile together.

Trial-to-trial reliability

The trial-to trial reliability of responses at BF was estimated for each neuron as the Fano Factor (FF). That is, the variance in the evoked response to the BF across trials, divided by the average evoked activity at BF.

Quantification of local BF variability

To assess the variability of frequency tuning within each imaging field, we computed the difference (in octaves) between each BF and the average BF of every other neuron in the imaging field, an approach similar to a recent study[26]. This analysis was performed independently on neurons from each of the three FRA classes, as well as on the three classes combined (i.e. all frequency-sensitive neurons). In this analysis, we included only imaging fields containing at least three single-peaked, three double-peaked and three complex neurons.

To compare the degree of local BF variability between mice and ferrets, it was necessary to account for differences in their hearing range and the length of their tonotopic gradient in A1. The mouse A1 is ~1 mm in length along the tonotopic gradient[14,15] and the hearing range of C57BL/6J mice at 10 weeks is 2-60 kHz[39,40], giving an A1 tonotopic map slope of 4.9 octaves/mm. In ferrets, the tonotopic gradient is ~3.5 mm[4,8] and the hearing range is ~36 Hz – 44 kHz[41], so the tonotopic gradient in A1 has a slope of 2.9 octaves/mm. For each imaging field, we first found the average BF across all the relevant neurons within the field (i.e. all neurons of a given FRA class). The expected BF range was then calculated around this average BF, given the tonotopic slopes above and the size of the imaging

715 field. The percentage of neurons having a BF within the expected range was used as a metric of
716 variability of local frequency tuning within the field for that neuronal class.
717
718 *Signal and noise correlations*
719 In keeping with previous studies[17,19], signal and noise correlations were computed between the evoked
720 responses of pairs of frequency-sensitive neurons recorded simultaneously. Briefly, noise correlations
721 were estimated by first normalizing each neuron's response to sounds presented on individual trials by
722 its signal response to that frequency/level combination. This normalization was obtained by
723 subtracting, from each single trial response, the average response to all tones presented at that
724 frequency/level combination. The noise correlation was then calculated across the normalized trial-
725 by-trial responses of two cells.
726
727 Signal correlations were calculated as the correlation between the trial-averaged responses of any two
728 neurons, minus the noise correlation computed for the neuronal pair.
729
730 *Analysing the effects of neuropil contamination*
731 Neuronal calcium traces extracted from two-photon imaging acquisitions can be contaminated by the
732 fluorescent signal coming from the pixels immediately surrounding each neuron. For this reason, it is
733 common practice to subtract from the neuronal trace what is known as the neuropil signal[51].
734
735 To test these effects, we calculated the BF of each neuron with and without neuropil subtraction, and
736 the results are presented in Figure 4-figure supplement 3. The results were examined separately for
737 the three FRA classes of neurons, and only for neurons that were frequency-sensitive (two-way
738 ANOVA, described above) both with and without neuropil correction. The presence of the neuropil
739 signal substantially changed the BF of some neurons (Figure 4-figure supplement 3A). Adding the
740 neuropil signal had a smaller change on the BF of single-peaked neurons (BFs; 0.48 ± 0.05 octaves;
741 mean ± SEM) than the BF of double-peaked neurons (BF_d; 0.76 ± 0.07 octaves; t-test; t = 3.36, p =
742 8.39×10^{-4}), peak 2 of double-peaked neurons (1.42 ± 0.09 octaves; t = 9.97, p = 2.25×10^{-21}), and the

743 BF of complex neurons (BF_c; 1.08 ± 0.11 octaves; t = 5.94, p = 6.19 x 10^{-09}). There was a trend for the
744 local variance in BF within an imaging field to be higher for double-peaked and complex neurons
745 when the neuropil was subtracted, but these trends were not statistically significant (Figure 4-figure
746 supplement 3B). When the BFs of "neuropil contaminated" neurons were mapped onto the common
747 template of A1, tonotopic organization was observed for single-peaked, double-peaked and complex
748 cells (Figure 4-figure supplement 3C). Unlike in the neuropil-corrected signals (Figure 4A3, 4B3,
749 4C3), the second frequency peak (peak 2) of double-peaked neurons also showed tonotopic
750 organization when the neurons contained neuropil contamination (Figure 4-figure supplement 3C3,
751 D3).
752
753 **In vivo electrophysiology**
754 *Data acquisition*
755 The animal preparation and anesthesia protocol was identical to the *in vivo* two-photon calcium
756 imaging procedures described above. Recordings were carried out in the left auditory cortex. An
757 Ag/AgCl external reference wire was inserted between the dura and the skull from the edge of
758 craniotomy. After durotomy, the brain surface was covered with a solution of 1.25% agarose in 0.9%
759 NaCl, and silicon oil was applied to the craniotomy regularly throughout recording.
760
761 A Neuropixels Phase 3a probe[52] was inserted orthogonally to the brain surface through the entire
762 depth of auditory cortex. Data were acquired at a 30 kHz sampling rate using SpikeGLX software
763 (https://github.com/billkarsh/SpikeGLX) and custom Matlab scripts.
764
765 *Sound presentation*
766 Electrophysiological recordings were made in a custom-built anechoic chamber. Stimuli were
767 presented binaurally via Panasonic RP-HV094E-K earphone drivers, coupled to otoscope speculae
768 inserted into each ear canal, and driven by a System 3 RP2.1 multiprocessor and headphone amplifier
769 (Tucker-Davis Technologies). The speculae were sealed in place with Otoform (GmbH). Speaker
770 calibration was performed as described above for imaging experiments. Pure tones (0.5 - 40 kHz,

771 0.45 octave spacing, 110 ms duration, 5 ms cosine onset and offset ramps) were presented at 5
772 intensity levels (40 - 80 dB SPL). Each frequency/intensity combination was presented for 20
773 repetitions, in pseudorandomized order, at a rate 1.37 Hz.
774
775 *Spike sorting*
776 The recorded signal was processed offline by first digitally highpass filtering at 150Hz. Common
777 average referencing was performed to remove noise across electrode channels[53]. Spiking activity was
778 then detected and clustered using Kilosort2 software (https://github.com/MouseLand/Kilosort2)[54].
779 Responses from single neurons were manually curated using Phy (https://github.com/cortex-lab/phy),
780 if they had stereotypical spike shapes with low variance, and their autocorrelation spike histogram
781 showed a clear refractory period. Spikes from a given cluster were often measurable on 4-6
782 neighboring electrode channels, facilitating the isolation of single units. Only well isolated single unit
783 were included in subsequent analyses.
784
785 *Current source density analysis*
786 In order to directly compare the properties of neurons recorded with Neuropixels probes to those
787 measured with two-photon calcium imaging, we aimed to isolate single units from cortical Layers 2/3
788 in our electrophysiological recordings. To this aim, we identified the boundary between Layer 1 and
789 Layer 2/3 in each recording penetration based on current source density maps.
790 The Local Field Potential (LFP) signal was isolated from the signal on each recording channel by
791 bandpass filtering from 2-300 Hz, and notch filtering at 50 Hz to remove potential electrical noise.
792 The evoked LFP trace was defined as time-series of the LFP signal starting 50 ms before tone
793 presentation, and ending 50 ms after sound offset. This trace was averaged across repeated
794 presentations and intensity levels for each tone frequency, and the frequency eliciting the strongest
795 evoked LFP deflection was determined to be the best frequency for the channel. The current source
796 density map of the recording was then derived as the derivative of the evoked LFP trace in response to
797 tones presented at BF (± 0.3 octaves), for all channels aligned vertically along the electrode. For all

A1 penetrations, there was a clear reversal in LFP polarity at the boundary between Layer 1 and Layers 2/3, as previously described[55,56].

Calculating the best frequency of single units

Single units were identified on channels from the upper border of Layers 2/3 (based on current source density analysis) to depths 400 µm below this border. The evoked spike rate for each neuron on each trial was calculated as the sum of spikes from tone onset to offset. The proportion of frequency-sensitive neurons (two-way ANOVA; $p < 0.05$), BF, and FRA classifications of these evoked spike responses were calculated as described above for calcium imaging data.

Acknowledgements

We are grateful to Prof Patrick Kanold for his advice and help in setting up our initial two-photon calcium imaging experiments in ferrets. Thanks to Dr Ben Willmore for assistance with electrophysiological experiments. Thanks also to the MICRON imaging facility (http://micronoxford.com, supported by Wellcome Strategic Awards 091911/B/10/Z and 107457/Z/15/Z) for technical advice and access to equipment. This work was supported by a BBSRC New Investigator Award (BB/M010929/1) and a DPAG Early Career Fellowship (University of Oxford) to KMMW, a Christopher Welch Scholarship (Oxford University Press) to AZI, a Newton-Abraham Scholarship (University of Oxford) to MP, and a Wellcome Principal Research Fellowship to AJK (WT076508AIA, WT108369/Z/2015/Z).

Author Contributions

KMMW and MP designed the experiment. AZI, KMMW, MP and QG collected two-photon calcium imaging data in ferrets. MP collected data in mice. AZI, KMMW and QG collected electrophysiological data in ferrets. AZI and QG performed histology and confocal imaging. AZI,

KMMW, MP and QG analyzed the data. KMMW, MP and QG wrote the manuscript. JCD and AJK provided technical assistance and edited the manuscript. AJK and KMMW provided funding.

Competing Interests statement

The authors declare no competing financial interests.

References

1. Winer, J. A. & Lee, C. C. The distributed auditory cortex. *Hear. Res.* **229**, 3–13 (2007).
2. Merzenich, M. M. & Brugge, J. F. Representation of the cochlear partition on the superior temporal plane of the macaque monkey. *Brain Res.* **50**, 275–296 (1973).
3. Hind, J. E. An electrophysiological determination of tonotopic organization in auditory cortex of cat. *J. Neurophysiol.* **16**, 475–89 (1953).
4. Kelly, J. B., Judge, P. W. & Phillips, D. P. Representation of the cochlea in primary auditory cortex of the ferret (Mustela putorius). *Hear. Res.* **24**, 111–5 (1986).
5. Steffen, H., Simonis, C., Thomas, H., Tillein, J. & Scheich, H. Auditory cortex: Multiple fields, their architectonics and connections in the Mongolian Gerbil. in *Auditory Pathway* 223–228 (Springer US, 1988). doi:10.1007/978-1-4684-1300-7_33
6. Sally, S. L. & Kelly, J. B. Organization of auditory cortex in the albino rat: sound frequency. *J. Neurophysiol.* **59**, 1627–1638 (1988).
7. Imaizumi, K. *et al.* Modular functional organization of cat anterior auditory field. *J. Neurophysiol.* **92**, 444–457 (2004).
8. Bizley, J. K., Nodal, F. R., Nelken, I. & King, A. J. Functional organization of ferret auditory cortex. *Cereb. Cortex* **15**, 1637–1653 (2005).
9. Recanzone, G. H., Schreiner, C. E., Sutter, M. L., Beitel, R. E. & Merzenich, M. M. Functional organization of spectral receptive fields in the primary auditory cortex of the owl monkey. *J.*

Comp. Neurol. **415**, 460–481 (1999).

10. Nelken, I. *et al.* Responses of auditory cortex to complex stimuli: functional organization revealed using intrinsic optical signals. *J. Neurophysiol.* **99**, 1928–1941 (2008).

11. Bendor, D. & Wang, X. Neural response properties of primary, rostral, and rostrotemporal core felds in the auditory cortex of marmoset monkeys. *J. Neurophysiol.* **100**, 888–906 (2008).

12. Goldstein, M. H., Abeles, M., Daly, R. L. & McIntosh, J. Functional architecture in cat primary auditory cortex: tonotopic organization. *J. Neurophysiol.* **33**, 188–197 (1970).

13. Hackett, T. A., Rinaldi Barkat, T., O'Brien, B. M. J., Hensch, T. K. & Polley, D. B. Linking topography to tonotopy in the mouse auditory thalamocortical circuit. *J. Neurosci.* **31**, 2983–2995 (2011).

14. Guo, W. *et al.* Robustness of cortical topography across fields, laminae, anesthetic states, and neurophysiological signal types. *J. Neurosci.* **32**, 9159–9172 (2012).

15. Stiebler, I., Neulist, R., Fichtel, I. & Ehret, G. The auditory cortex of the house mouse: left-right differences, tonotopic organization and quantitative analysis of frequency representation. *J. Comp. Physiol. A Sensory, Neural, Behav. Physiol.* **181**, 559–571 (1997).

16. Bandyopadhyay, S., Shamma, S. a & Kanold, P. O. Dichotomy of functional organization in the mouse auditory cortex. *Nat. Neurosci.* **13**, 361–368 (2010).

17. Rothschild, G., Nelken, I. & Mizrahi, A. Functional organization and population dynamics in the mouse primary auditory cortex. *Nat. Neurosci.* **13**, 353–360 (2010).

18. Issa, J. B. *et al.* Multiscale optical ca2+ imaging of tonal organization in mouse auditory cortex. *Neuron* **83**, 944–959 (2014).

19. Panniello, M., King, A. J., Dahmen, J. C. & Walker, K. M. M. Local and global spatial organization of interaural level difference and frequency preferences in auditory cortex. *Cereb. Cortex* **28**, (2018).

20. Romero, S. *et al.* Cellular and widefield imaging of sound frequency organization in primary and higher-order fields of the mouse auditory cortex. *Cereb. Cortex* Epub (2019). doi:10.1093/cercor/bhz190

21. Kerr, J. N. D. *et al.* Spatial organization of neuronal population responses in layer 2/3 of rat

880 barrel cortex. *J. Neurosci.* **27**, 13316–28 (2007).

881 22. Sato, T. R., Gray, N. W., Mainen, Z. F. & Svoboda, K. The functional microarchitecture of the
882 mouse barrel cortex. *PLoS Biol.* **5**, e189 (2007).

883 23. Bonin, V., Histed, M. H., Yurgenson, S. & Reid, R. C. Local diversity and fine-scale
884 organization of receptive fields in mouse visual cortex. *J. Neurosci.* **31**, 18506–21 (2011).

885 24. Kanold, P. O., Nelken, I. & Polley, D. B. Local versus global scales of organization in auditory
886 cortex. *Trends Neurosci.* **37**, 502–510 (2014).

887 25. Winkowski, D. E. & Kanold, P. O. Laminar transformation of frequency organization in
888 auditory cortex. *J. Neurosci.* **33**, 1498–1508 (2013).

889 26. Tischbirek, C. H. *et al.* In vivo functional mapping of a cortical column at single-neuron
890 resolution. *Cell Rep.* (2019). doi:10.1016/j.celrep.2019.04.007

891 27. Vasquez-Lopez, S. A. *et al.* Thalamic input to auditory cortex is locally heterogeneous but
892 globally tonotopic. *Elife* **6**, 1–18 (2017).

893 28. Ohki, K., Chung, S., Ch'ng, Y. H., Kara, P. & Reid, R. C. Functional imaging with cellular
894 resolution reveals precise microarchitecture in visual cortex. *Nature* **433**, 597–603 (2005).

895 29. Lee, K. S., Huang, X. & Fitzpatrick, D. Topology of on and off inputs in visual cortex enables
896 an invariant columnar architecture. *Nature* **533**, 90–94 (2016).

897 30. Wilson, D. E. *et al.* GABAergic neurons in ferret visual cortex participate in functionally
898 specific networks. *Neuron* **93**, 1058-1065.e4 (2017).

899 31. Zeng, H. *et al.* Local homogeneity of tonotopic organization in the primary auditory cortex of
900 marmosets. *Proc. Natl. Acad. Sci.* **116**, 3239–3244 (2019).

901 32. Linden, J. F. & Schreiner, C. E. Columnar transformations in auditory cortex? A comparison
902 to visual and somatosensory cortices. *Cereb. Cortex* **13**, 83–89 (2003).

903 33. Ahrens, M. B., Linden, J. F. & Sahani, M. Nonlinearities and contextual influences in auditory
904 cortical responses modeled with multilinear spectrotemporal methods. *J. Neurosci.* **28**, 1929–
905 42 (2008).

906 34. Sadagopan, S. & Wang, X. Nonlinear spectrotemporal interactions underlying selectivity for
907 complex sounds in auditory cortex. *J. Neurosci.* **29**, 11192–202 (2009).

908 35. Sutter, M. L. & Schreiner, C. E. Physiology and topography of neurons with multipeaked
909 tuning curves in cat primary auditory cortex. *J. Neurophysiol.* **65**, 1207–1226 (1991).
910 36. Kadia, S. C. & Wang, X. Spectral Integration in A1 of Awake Primates: Neurons With Single-
911 and Multipeaked Tuning Characteristics. *J. Neurophysiol.* **89**, 1603–1622 (2003).
912 37. Turner, J. G., Hughes, L. F. & Caspary, D. M. Divergent response properties of layer-V
913 neurons in rat primary auditory cortex. *Hear. Res.* (2005). doi:10.1016/j.heares.2004.09.011
914 38. Hofer, S. B. *et al.* Differential connectivity and response dynamics of excitatory and inhibitory
915 neurons in visual cortex. *Nat. Neurosci.* **14**, 1045–1052 (2011).
916 39. Heffner, H. E. & Heffner, R. S. Hearing ranges of laboratory animals. *J. Am. Assoc. Lab.*
917 *Anim. Sci.* **46**, 20–2 (2007).
918 40. Ison, J. R., Allen, P. D. & O'Neill, W. E. Age-related hearing loss in C57BL/6J mice has both
919 frequency-specific and non-frequency-specific components that produce a hyperacusis-like
920 exaggeration of the acoustic startle reflex. *J. Assoc. Res. Otolaryngol.* **8**, 539–550 (2007).
921 41. Kelly, J. B., Kavanagh, G. L. & Dalton, J. C. H. Hearing in the ferret (Mustela putorius):
922 Thresholds for pure tone detection. *Hear. Res.* **24**, 269–275 (1986).
923 42. Romani, G. L., Williamson, S. J. & Kaufman, L. Tonotopic organization of the human
924 auditory cortex. *Science (80-.).* **216**, 1339–40 (1982).
925 43. Bizley, J. K., Walker, K. M. M., Silverman, B. W., King, A. J. & Schnupp, J. W. H.
926 Interdependent encoding of pitch, timbre, and spatial location in auditory cortex. *J. Neurosci.*
927 **29**, 2064–2075 (2009).
928 44. Andermann, M. L. *et al.* Chronic cellular imaging of entire cortical columns in awake mice
929 using microprisms. *Neuron* **80**, 900–913 (2013).
930 45. Barnstedt, O., Keating, P., Weissenberger, Y., King, A. J. & Dahmen, J. C. Functional
931 microarchitecture of the mouse dorsal inferior colliculus revealed through in vivo two-photon
932 calcium imaging. *J. Neurosci.* **35**, 10927–10939 (2015).
933 46. Cossell, L. *et al.* Functional organization of excitatory synaptic strength in primary visual
934 cortex. *Nature* **518**, 399–403 (2015).
935 47. Feng, L. & Wang, X. Harmonic template neurons in primate auditory cortex underlying

complex sound processing. *Proc. Natl. Acad. Sci. USA* 201607519 (2017). doi:10.1073/pnas.1607519114

48. Shoham, S., O'Connor, D. H. & Segev, R. How silent is the brain: is there a "dark matter" problem in neuroscience? *J. Comp. Physiol. A* **192**, 777–784 (2006).

49. Anderson, L. A., Christianson, G. B. & Linden, J. F. Mouse auditory cortex differs from visual and somatosensory cortices in the laminar distribution of cytochrome oxidase and acetylcholinesterase. *Brain Res.* **1252**, 130–142 (2009).

50. Dahmen, J. C., Hartley, D. E. H. & King, A. J. Stimulus-timing-dependent plasticity of cortical frequency representation. *J. Neurosci.* **28**, 13629–39 (2008).

51. Chen, T.-W. *et al.* Ultrasensitive fluorescent proteins for imaging neuronal activity. *Nature* **499**, 295–300 (2013).

52. Jun, J. J. *et al.* Fully integrated silicon probes for high-density recording of neural activity. *Nature* **551**, 232–236 (2017).

53. Ludwig, K. A. *et al.* Using a common average reference to improve cortical neuron recordings from microelectrode arrays. *J. Neurophysiol.* **101**, 1679–89 (2009).

54. Pachitariu, M., Steinmetz, N., Kadir, S., Carandini, M. & Harris, K. D. Kilosort : realtime spike-sorting for extracellular electrophysiology with hundreds of channels b c. 1–14 (2016).

55. Christianson, G. B., Sahani, M. & Linden, J. F. Depth-dependent temporal response properties in core auditory cortex. *J. Neurosci.* **31**, 12837–12848 (2011).

56. Szymanski, F. D., Rabinowitz, N. C., Magri, C., Panzeri, S. & Schnupp, J. W. H. The laminar and temporal structure of stimulus information in the phase of field potentials of auditory cortex. *J. Neurosci.* **31**, 15787–15801 (2011).

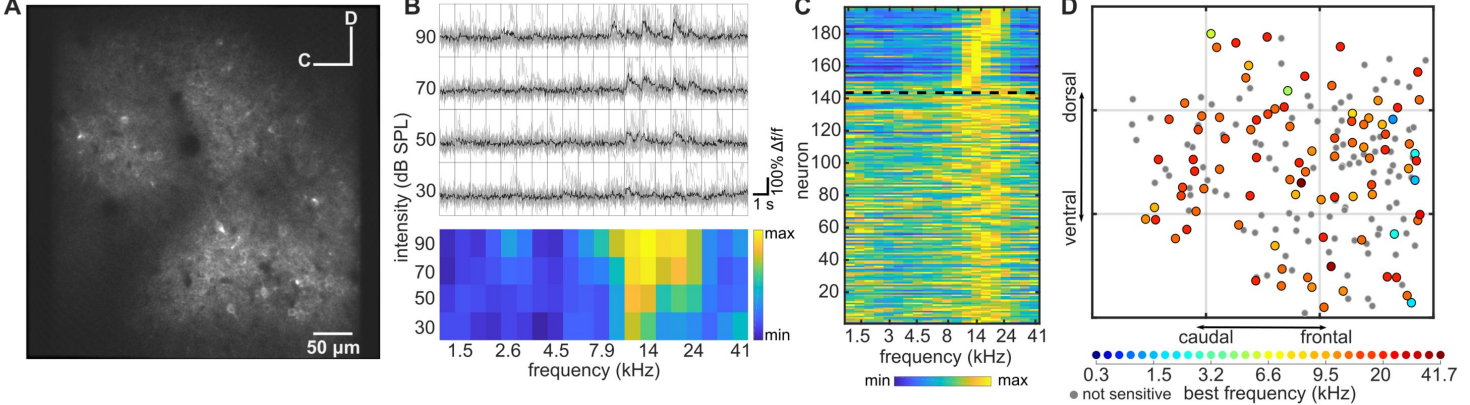
A
D
C
50 µm
B
90
70
50
30
1 s
100% Δf/f
intensity (dB SPL)
max
min
1.5 2.6 4.5 7.9 14 24 41
frequency (kHz)
C
neuron
180
160
140
120
100
80
60
40
20
1.5 3 4.5 8 14 24 41
frequency (kHz)
min
max
D
dorsal
ventral
caudal
frontal
0.3 1.5 3.2 6.6 9.5 20 41.7
not sensitive
best frequency (kHz)

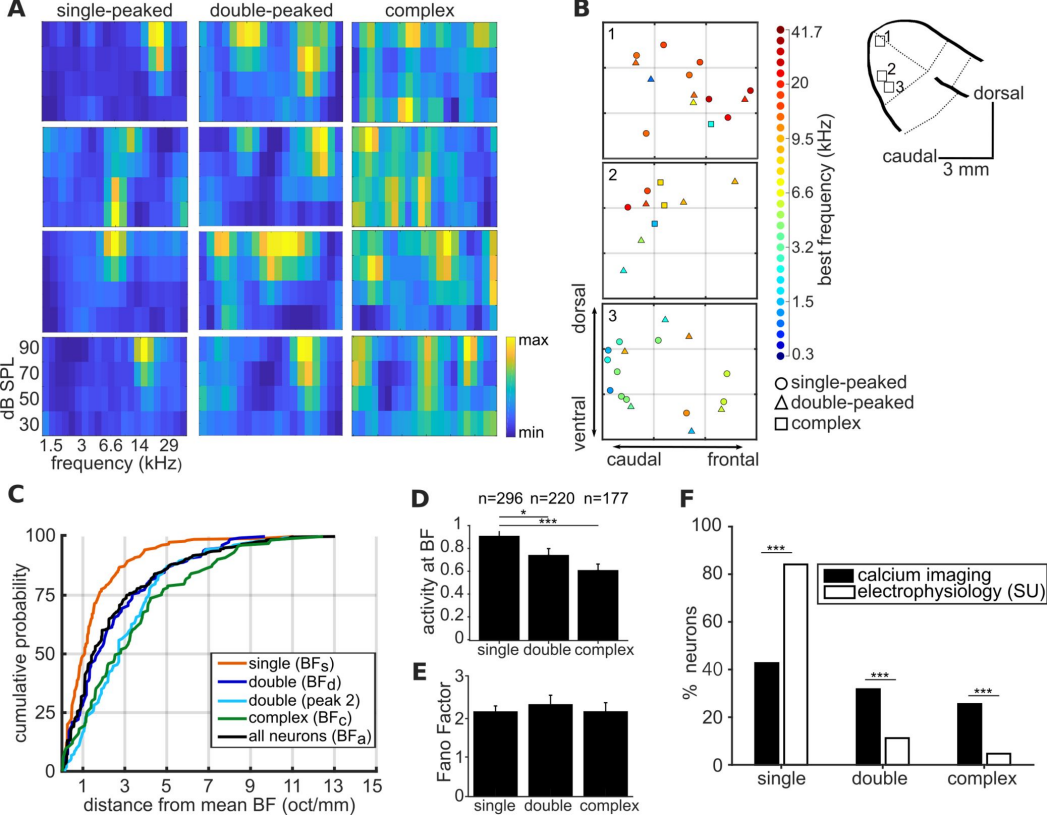
A
single-peaked
double-peaked
complex
dB SPL
90
70
50
30
1.5 3 6.6 14 29
frequency (kHz)
max
min
B
1
2
3
dorsal
ventral
caudal
frontal
41.7
20
9.5
6.6
3.2
1.5
0.3
best frequency (kHz)
single-peaked
double-peaked
complex
dorsal
caudal
3 mm
C
cumulative probability
distance from mean BF (oct/mm)
single (BFs)
double (BFd)
double (peak 2)
complex (BFc)
all neurons (BFa)
D
n=296 n=220 n=177
activity at BF
single double complex
E
Fano Factor
single double complex
F
% neurons
calcium imaging
electrophysiology (SU)
single
double
complex

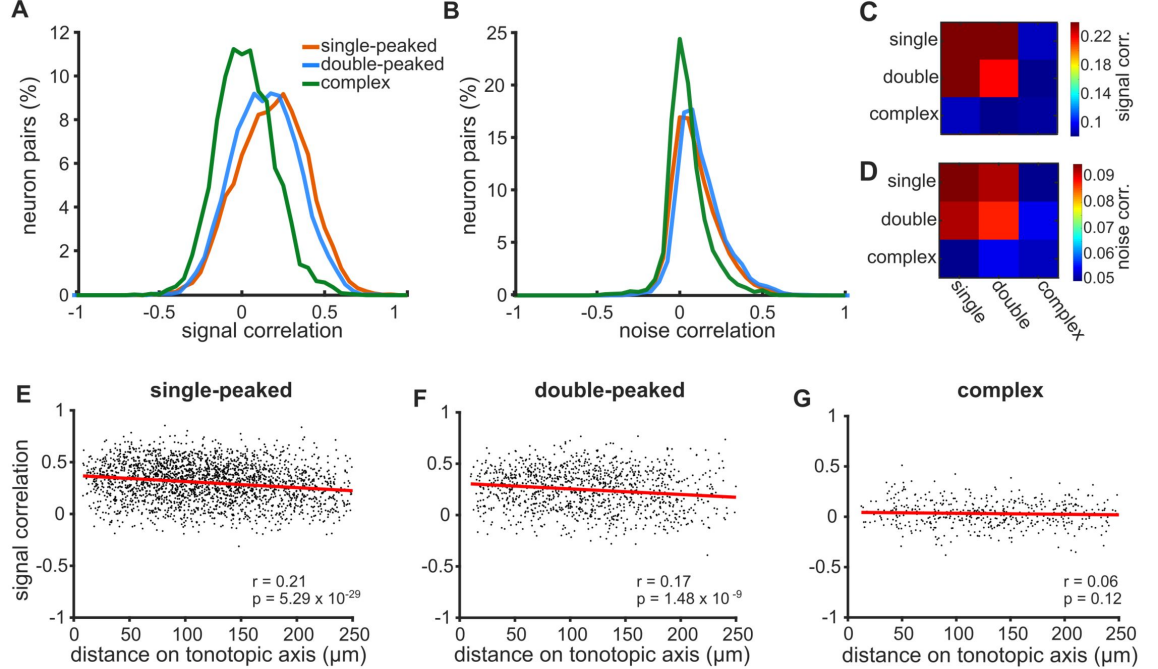
A
B
C
D
E
F
G
single-peaked
double-peaked
complex
neuron pairs (%)
signal correlation
noise correlation
signal corr.
noise corr.
single
double
complex
r = 0.21
p = 5.29 x 10-29
r = 0.17
p = 1.48 x 10-9
r = 0.06
p = 0.12
distance on tonotopic axis (μm)

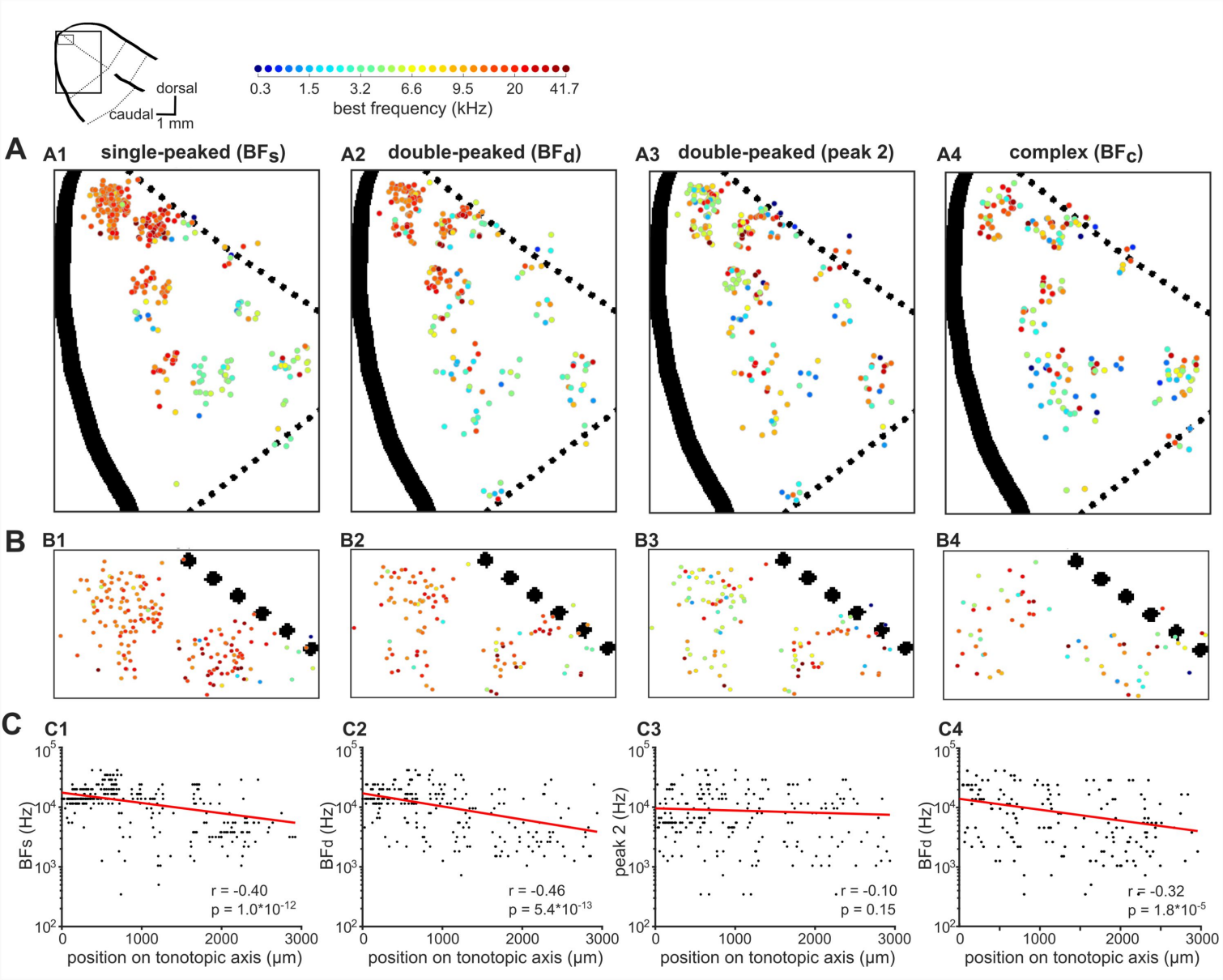
dorsal
caudal
1 mm
0.3
1.5
3.2
6.6
9.5
20
41.7
best frequency (kHz)
A
A1
single-peaked (BFs)
A2
double-peaked (BFd)
A3
double-peaked (peak 2)
A4
complex (BFc)
B
B1
B2
B3
B4
C
C1
C2
C3
C4
BFs (Hz)
BFd (Hz)
peak 2 (Hz)
position on tonotopic axis (µm)
r = -0.40
p = 1.0*10-12
r = -0.46
p = 5.4*10-13
r = -0.10
p = 0.15
r = -0.32
p = 1.8*10-5

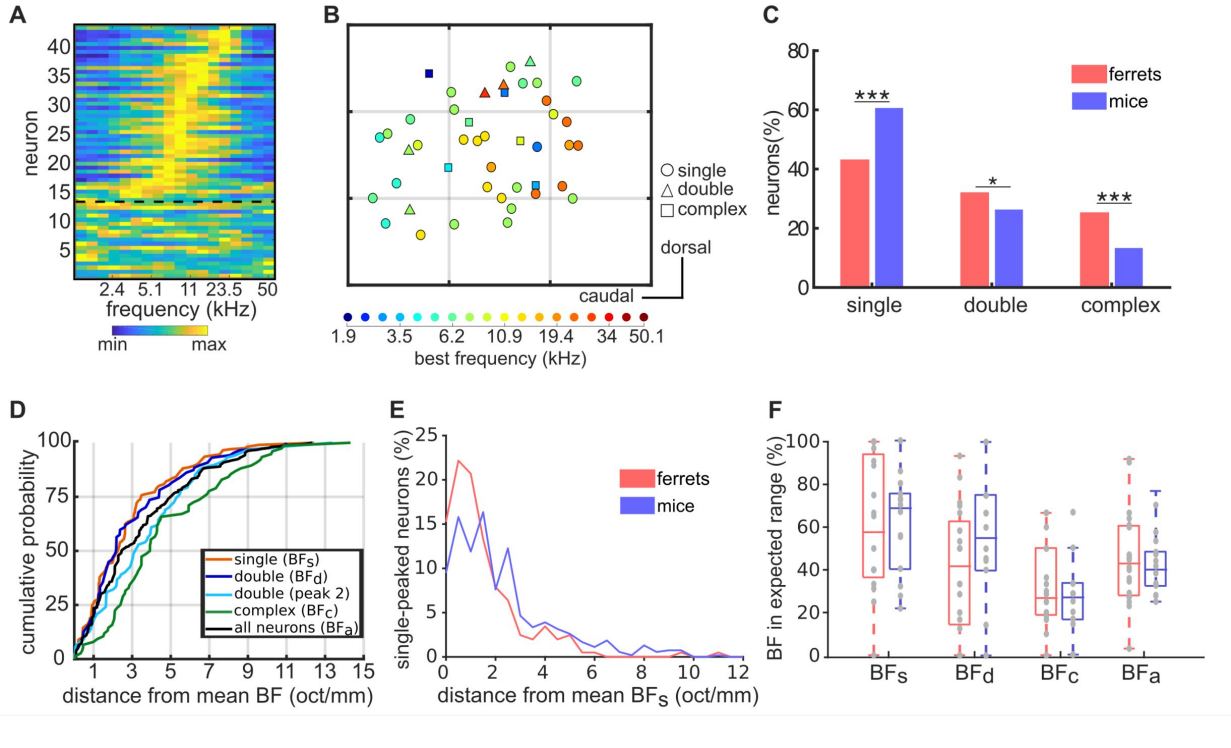
A
neuron
40
35
30
25
20
15
10
5
2.4 5.1 11 23.5 50
frequency (kHz)
min
max
B
single
double
complex
dorsal
caudal
1.9 3.5 6.2 10.9 19.4 34 50.1
best frequency (kHz)
C
neurons(%)
80
60
40
20
0
ferrets
mice
***
*
***
single
double
complex
D
cumulative probability
100
75
50
25
0
1 3 5 7 9 11 13 15
distance from mean BF (oct/mm)
single (BFs)
double (BFd)
double (peak 2)
complex (BFc)
all neurons (BFa)
E
single-peaked neurons (%)
25
20
15
10
5
0
0 2 4 6 8 10 12
distance from mean BFs (oct/mm)
ferrets
mice
F
BF in expected range (%)
100
80
60
40
20
0
BFs
BFd
BFc
BFa

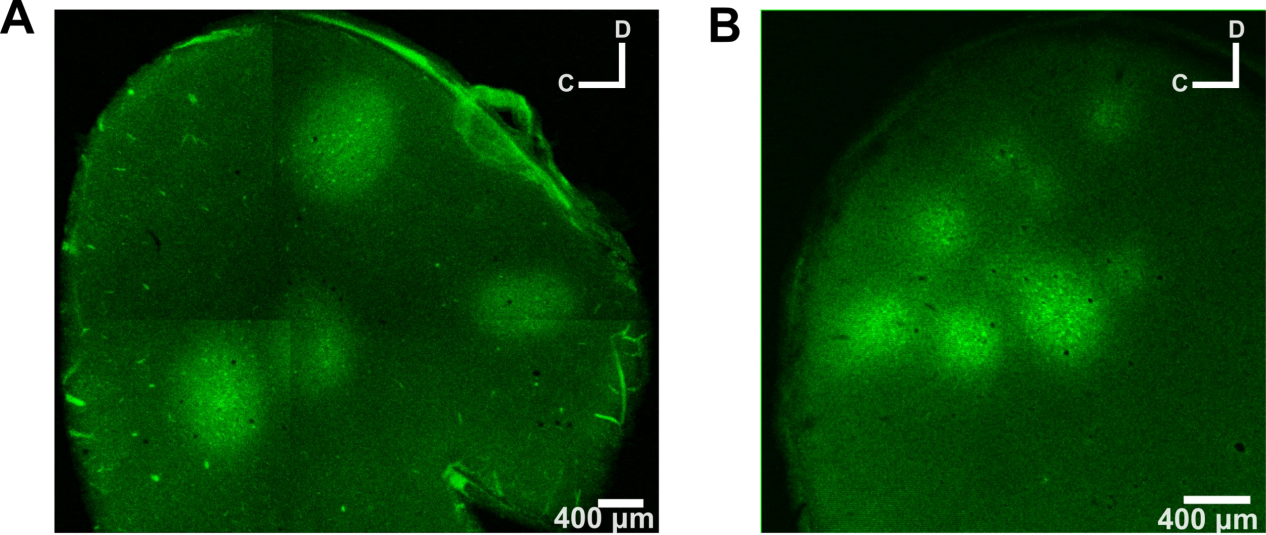
A
D
C
400 µm
B
D
C
400 µm

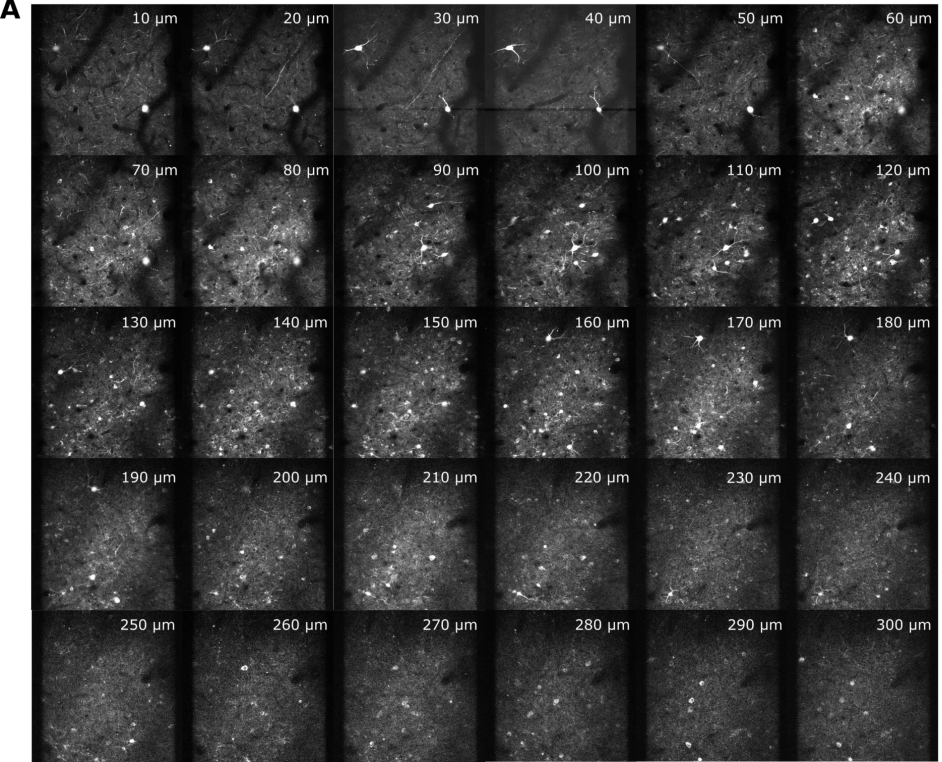
A
10 µm
20 µm
30 µm
40 µm
50 µm
60 µm
70 µm
80 µm
90 µm
100 µm
110 µm
120 µm
130 µm
140 µm
150 µm
160 µm
170 µm
180 µm
190 µm
200 µm
210 µm
220 µm
230 µm
240 µm
250 µm
260 µm
270 µm
280 µm
290 µm
300 µm

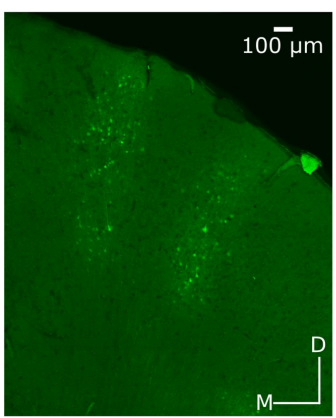
B
100 µm
D
M

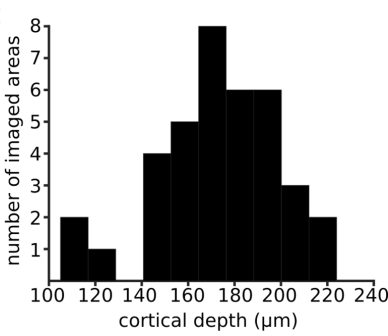
C
number of imaged areas
1
2
3
4
5
6
7
8
100
120
140
160
180
200
220
240
cortical depth (µm)

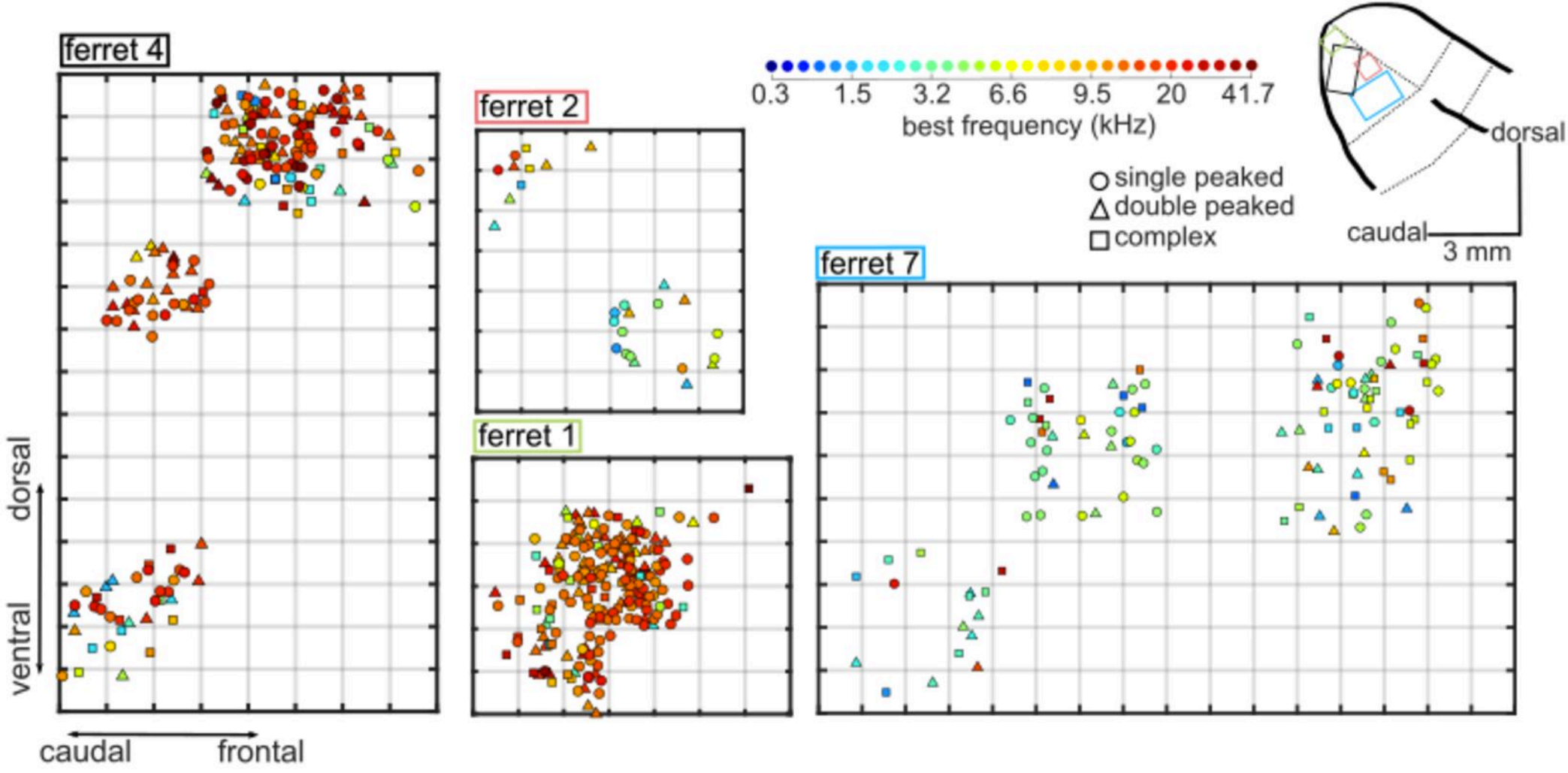
ferret 4
ferret 2
ferret 1
ferret 7
0.3
1.5
3.2
6.6
9.5
20
41.7
best frequency (kHz)
single peaked
double peaked
complex
dorsal
caudal
3 mm
dorsal
ventral
caudal
frontal

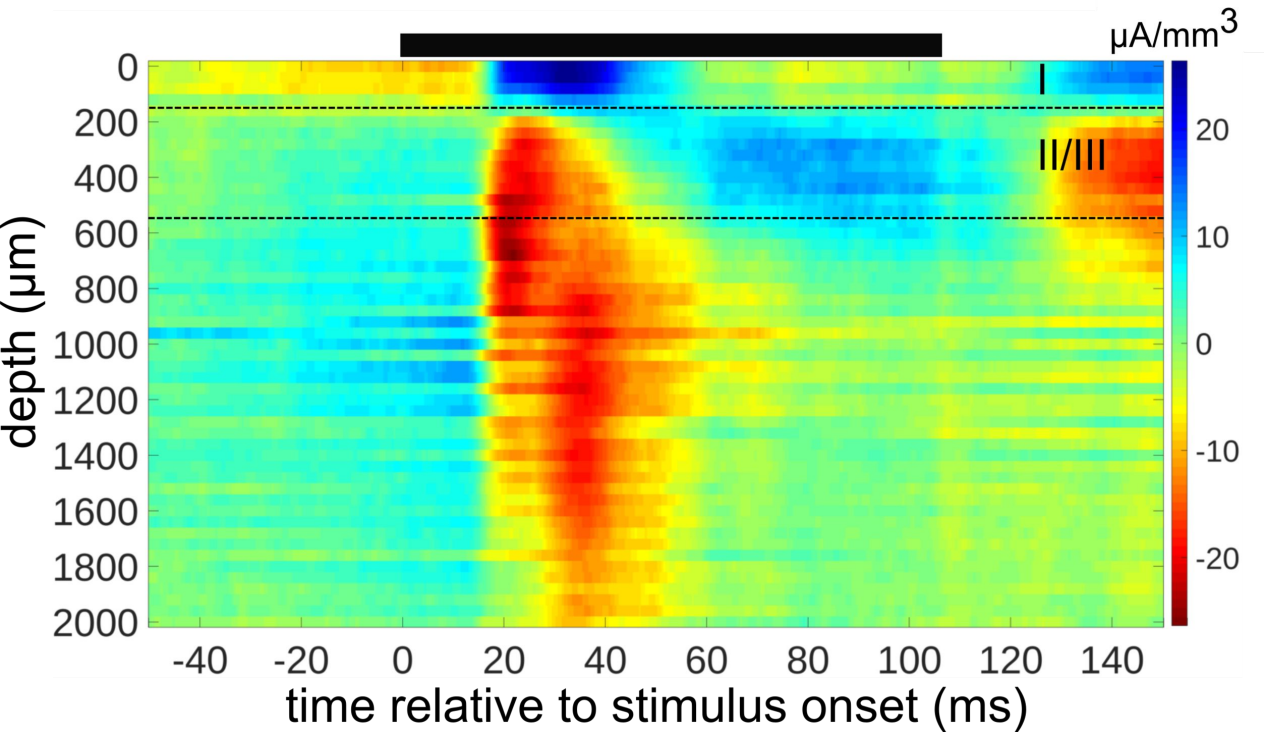
μA/mm3
I
II/III
depth (μm)
0
200
400
600
800
1000
1200
1400
1600
1800
2000
20
10
0
-10
-20
-40
-20
0
20
40
60
80
100
120
140
time relative to stimulus onset (ms)

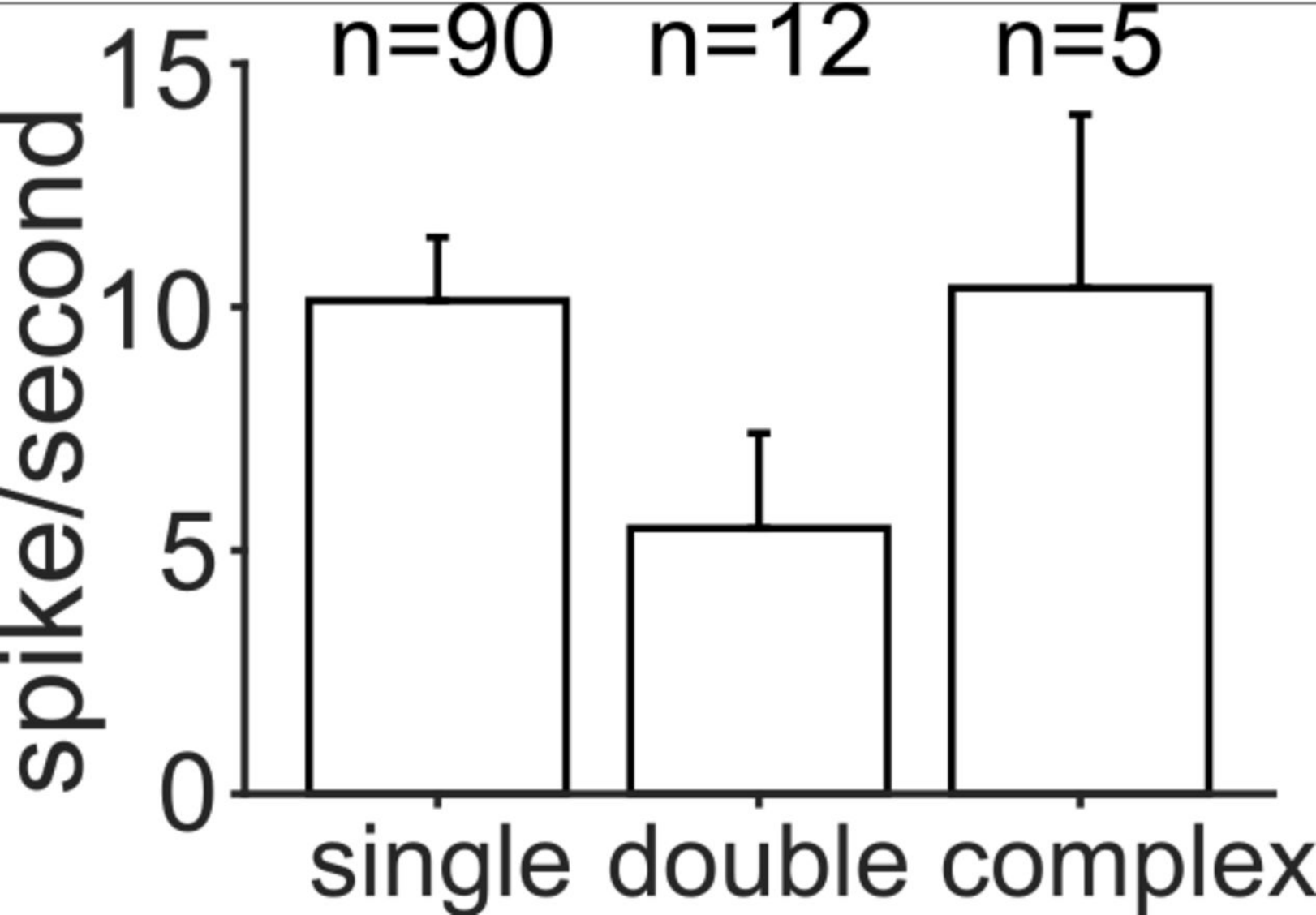
n=90
n=12
n=5
15
10
5
0
spike/second
single
double
complex

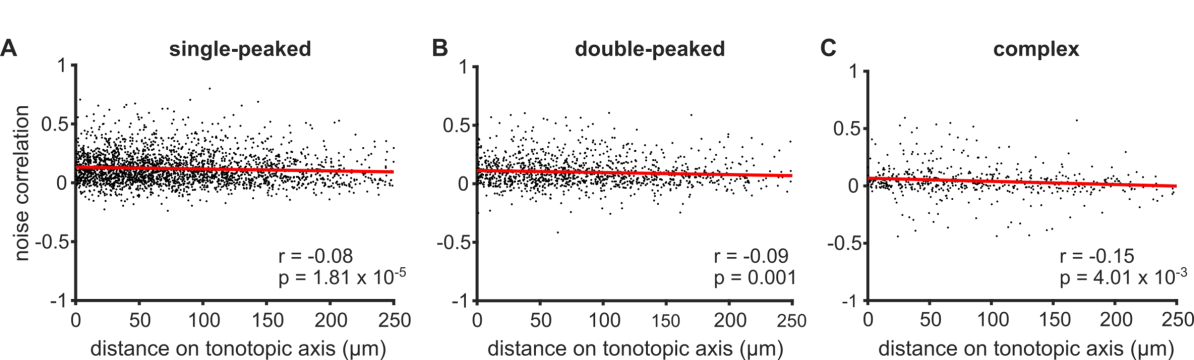
A
single-peaked
noise correlation
1
0.5
0
-0.5
-1
r = -0.08
p = 1.81 x 10-5
0
50
100
150
200
250
distance on tonotopic axis (µm)
B
double-peaked
r = -0.09
p = 0.001
C
complex
r = -0.15
p = 4.01 x 10-3

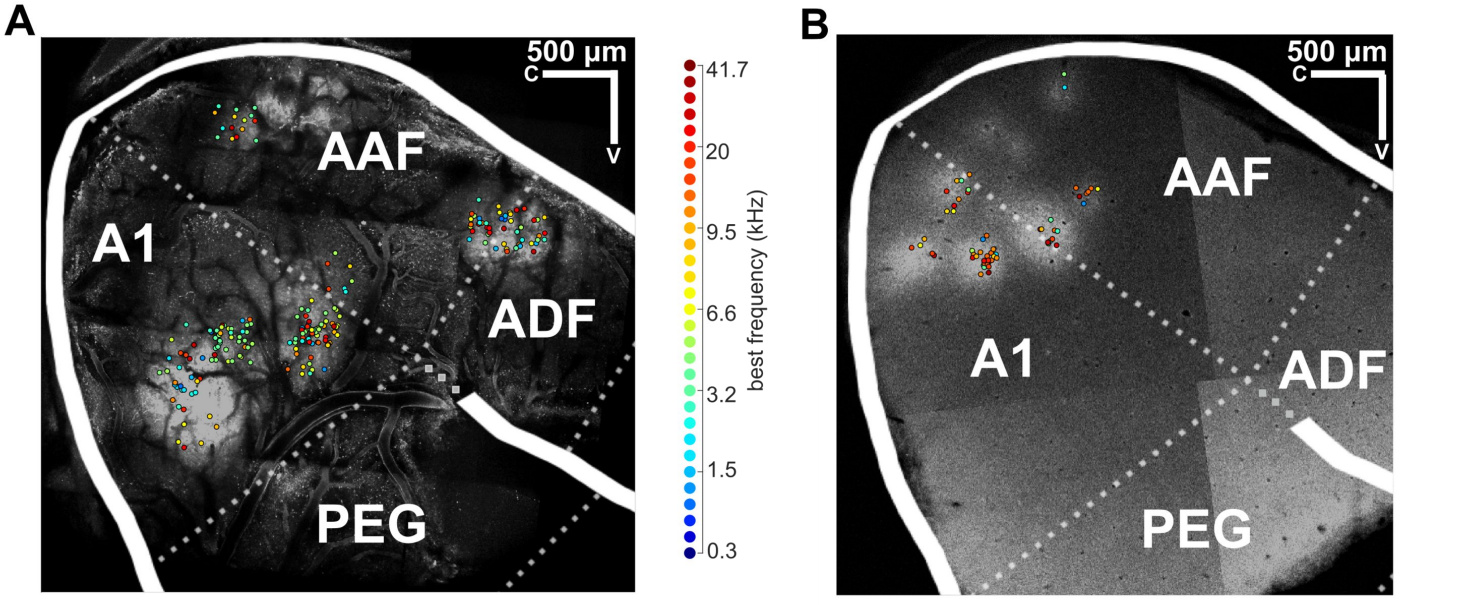
A
500 µm
C
V
AAF
A1
ADF
PEG
41.7
20
9.5
6.6
3.2
1.5
0.3
best frequency (kHz)
B
500 µm
C
V
AAF
A1
ADF
PEG

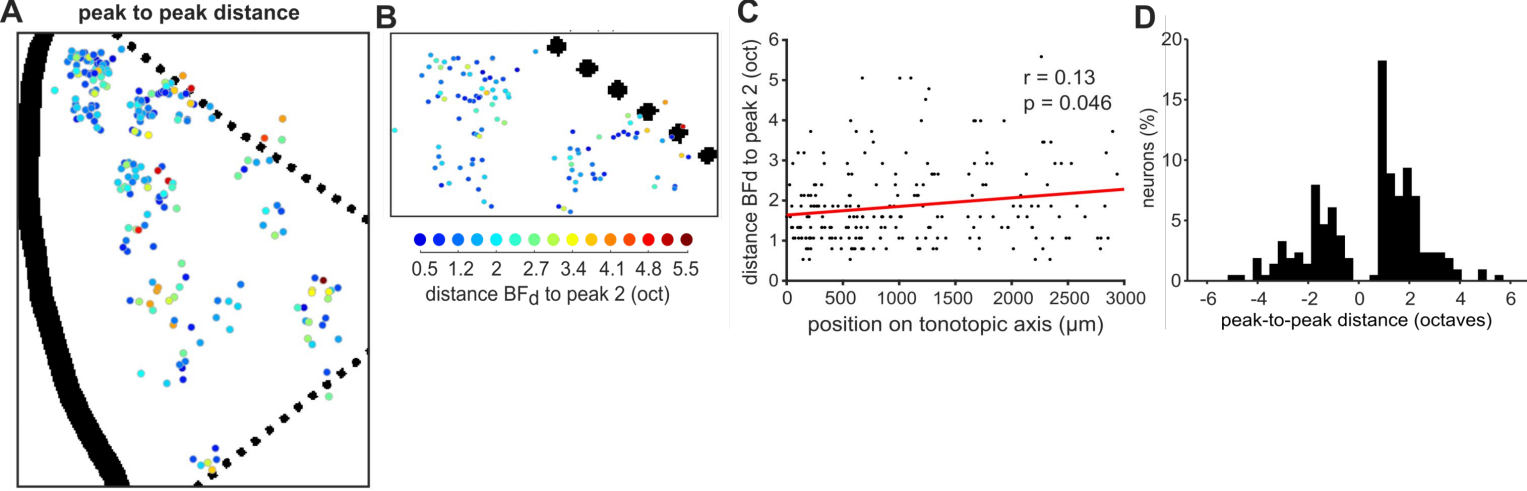
A
peak to peak distance
B
0.5 1.2 2 2.7 3.4 4.1 4.8 5.5
distance BFd to peak 2 (oct)
C
r = 0.13
p = 0.046
distance BFd to peak 2 (oct)
position on tonotopic axis (µm)
D
neurons (%)
peak-to-peak distance (octaves)

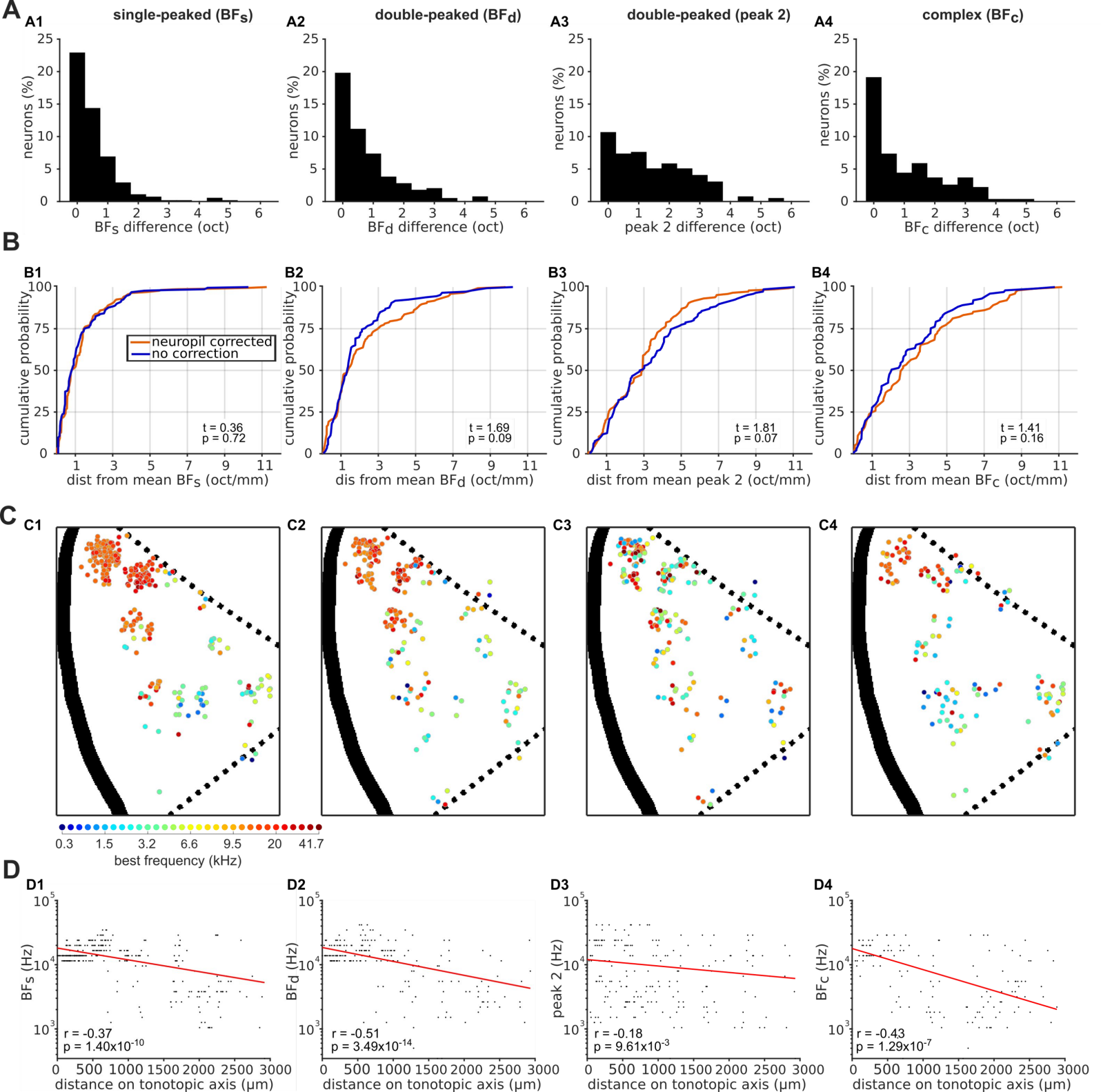
A
A1
single-peaked (BFs)
A2
double-peaked (BFd)
A3
double-peaked (peak 2)
A4
complex (BFc)
neurons (%)
BFs difference (oct)
BFd difference (oct)
peak 2 difference (oct)
BFc difference (oct)
B
B1
B2
B3
B4
cumulative probability
neuropil corrected
no correction
t = 0.36
p = 0.72
t = 1.69
p = 0.09
t = 1.81
p = 0.07
t = 1.41
p = 0.16
dist from mean BFs (oct/mm)
dis from mean BFd (oct/mm)
dist from mean peak 2 (oct/mm)
dist from mean BFc (oct/mm)
C
C1
C2
C3
C4
0.3
1.5
3.2
6.6
9.5
20
41.7
best frequency (kHz)
D
D1
D2
D3
D4
BFs (Hz)
BFd (Hz)
peak 2 (Hz)
BFc (Hz)
r = -0.37
p = 1.40x10-10
r = -0.51
p = 3.49x10-14
r = -0.18
p = 9.61x10-3
r = -0.43
p = 1.29x10-7
distance on tonotopic axis (µm)